Western Graduate&PostdoctoralStudies

Western University

Scholarship@Western

Electronic Thesis and Dissertation Repository

12-15-2015 12:00 AM

Intracellular Acidification in Brain Tumors Induced by Topiramate : In-Vivo Detection Using Chemical Exchange Saturation Transfer Magnetic Resonance Imaging

Kamini Y. Marathe
The University of Western Ontario

Supervisor
Dr. Robert Bartha
The University of Western Ontario

Follow this and additional works at: https://ir.lib.uwo.ca/etd

Part of the Medical Biophysics Commons

Recommended Citation

Topiramate Induced Intracellular acidification in brain tumors : In-vivo detection using chemical exchange saturation transfer magnetic resonance imaging

(Thesis format: Integrated Article)

by

Kamini Y. Marathe

Graduate Program in Medical Biophysics

A thesis submitted in partial fulfillment
of the requirements for the degree of
Master of science

The School of Graduate and Postdoctoral Studies
The University of Western Ontario
London, Ontario, Canada

Abstract

Glioblastoma Multiforme (GBM) is the most aggressive and malignant form of primary brain tumor. In many tumors, increased intracellular pH (pH_i) is a hallmark of aggressiveness. This increased pH_i has been shown to be related to cell proliferation and evasion of apoptosis as well as resistance to chemotherapy. As such, monitoring pH_i and the tumor pH_i response to pharmacologic challenge, may aid in treatment planning and patient management for this deadly cancer. A magnetic resonance imaging (MRI) method called Chemical Exchange Saturation Transfer (CEST) has been used to detect changes in pH_i. Our group has recently developed a CEST technique called amine and amide concentration independent detection (AACID), which was shown to be sensitive to pH_i changes induced by the anticancer drug, lonidamine (LND). However, LND is not currently approved for use in humans. Our objective was to demonstrate that topiramate (TPM), an antiepileptic drug that is well tolerated in humans, could also induce tumor acidification. The goal this thesis was to quantify the changes in pH_i induced by a single dose of TPM in a mouse model of brain tumor. CEST spectra were acquired using a 9.4T MRI scanner, before and 75 minutes after administration of TPM (dose: 120 mg/kg). A significant increase in the AACID CEST effect was observed within brain tumors with no change observed in contralateral tissue. The increase in AACID CEST corresponds to tumor acidification as expected. Therefore TPM induced a rapid measurable metabolic change in tumors that could provide valuable insight into cancer aggressiveness and aid in tumor detection.

Keywords: MRI- Magnetic Resonance Imaging, CEST- Chemical Exchange Saturation Transfer, pH_i-Intracellular pH, APT- Amide Proton Transfer, TPM- Topiramate, AACID- Amine and Amide Concentration Independent Detection, GBM- Glioblastoma Multiforme

Co-Authorship

The thesis presented here consists of one study and contains material from posters that have been previously presented. My graduate work was supervised by Dr. Robert Bartha who designed the study, guided the interpretation of results, provided project motivation, and edited the manuscript. Data were acquired by Dr. Alex Li. The original MATLAB code used for data analysis was provided by Dr. Nevin McVicar. Dr. Susan Meakin provided the U87 tumor cells and Miranda Bellyou (Animal Technologist) implanted the tumor cells to produce the mouse model. Dr. Mojmir Suchy helped with the preparation of injectable Topiramate. As the primary author of this thesis, I was responsible for assisting in experimental design, all data analyses, interpretation of the data, and writing the first draft of the manuscript as well as incorporating ongoing suggestions.

For my Parents

Mr. Jayram Jadhav and Mrs. Pushpa Jadhav

Acknowledgments

First, I would like to thank my supervisor Dr. Robert Bartha. I wouldn't have completed my graduate studies without his support and guidance. I will always remember his words of encouragement when I felt that I won't be able to pursue my studies further. He has been an important mentor that I have met during the years of my educational journey. His welcoming and enthusiastic nature always made me feel comfortable to go knock on his office door anytime and discuss the issues or results regarding my work. Thank you for being patient, accessible, and for providing valuable guidance.

I would also like to thank my committee members, Dr. Paula Foster and Dr. Timothy Scholl for their suggestions and advice.

I deeply express my gratitude towards Nevin McVicar and Alex Li for their discussions on basic science of this thesis and guidance in data analysis. Nevin always pointed me towards new directions of thinking which led me to achieve the answers to my questions. Alex always guided me through the jungle of Matlab programming needed for this study. These two fellows have played an important role in my journey at Robarts.

I would also like to thank –Mojmir Suchy, Dr. Susan Meakin and Miranda Bellyou for their contribution in completion of this project.

I would like to thank, my cube mate Jonathan Snir for his words of encouragement, Sandy Goncalves for her great suggestions on the presentations during my graduate study and all the other great members in Dr. Bartha's group.

Thank you to my husband, Yogesh who always stood by me throughout my degree without losing his patience. He was the one who always helped me to pass through my anxiety before any presentation and helped me to stick to my goals.

My mom and my in-laws deserve special thanks for their confidence in me and constant support as they came to stay with me and helped me in taking care of my kids when I needed them the most.

Finally, but not the least I would like to thank my family friends for showing interest in my work, for asking me how far I am in my project and most importantly for asking, 'so, when are you going to defend!', almost every time we met.

Table of Contents

List of Figures

List of Appendices

List of Acronyms and Symbols

MRI	Magnetic Resonance Imaging
CEST	Chemical Exchange Saturation Transfer
AACID	Amine Amide Concentration independent Detection
WHO	World Health Organisation
CNS	Central Nervous system
GBM	Glioblastoma Multiforme
PTEN	Phosphate and Tensin homolog
EGFR	Epidermal Growth Factor Receptor
VPF	Vascular Permeability Factor
VEGF	Vascular Endothelium Growth Factor
pH_i	Intracellular pH
pH_e	Extracellular pH
ATP	Adenosine Triphosphate
CA	Carbonic Anhydrase, Contrast Agent
AQP	Aquaporin
CAI	Carbonic anhydrase Inhibitor
DCE- MRI	Dynamic Contrast Enhanced magnetic Resonance Imaging
T1	Longitudinal Relaxation Time
T2	Transverse Relaxation Time
PARACEST	Paramagnetic CEST
PET	Positron emission Tomography
FDG	Fluorodeoxyglucose
CT	Computed Tomography
MRS	Magnetic Resonance Spectroscopy
CR	Creatine
TCHO	Total Choline
LAC	Lactate
NAA	N- acetyl aspartate
TCR	Total Creatine

L	Lipid
DWI	Diffusion Weighted Imaging
ADC	Apparent- Diffusion Coefficient
MT	Magnetization Transfer
MTR	Magnetization Transfer Ratio
APT	Amide Proton Transfer
μs	microsecond
ms	millisecond
K	Exchange rate
K_{ws}	Water-solute exchange rate
K_{sw}	Solute-water exchange rate
M	Moles
μM	micromoles
mM	millimoles
ω	Resonance frequency
$\Delta\omega$	Frequency difference
R1	Longitudinal relaxation rate
RF	Radio Frequency
NMR	Nuclear Magnetic Resonance
ppm	parts per million
9.4 T	9.4 Tesla
B_0	The static magnetic field
TR	Repetition Time
TE	Echo Time
ETL	Echo Train Length
FOV	Field- of- View

Chapter 1

1 Brain Tumors

1.1 Introduction

The work presented in this thesis uses high field magnetic resonance imaging (MRI) and a novel chemical exchange saturation (CEST) method called amine and amide concentration independent detection (AACID) for the quantification of changes in intracellular pH (pH_i) caused by a single dose of the anticonvulsant drug topiramate.

This introductory chapter provides a framework for understanding the motivation, impact, and research methods presented in the subsequent chapters. Three principal subjects are described. The first is a description of cancer metabolism, and the cellular and chemical changes required to maintain the permissive microenvironment for disease progression. The second is a description of the methods, particularly MRI, used for disease diagnosis and treatment. Finally, the third is a description of the pH modulating mechanisms affected by the drug used in this thesis.

1.2 Impact

Cancer ranks third among the most costly diseases. The most recent estimated cost of cancer care in Canada in 2000 was $17.4 billion (www. omainsurance.com) [1]. Brain cancer is an abnormal growth of cells in the brain and is commonly called a brain tumor. There are two main types of brain tumors: primary and secondary. Primary brain tumors develop from the various cells of the brain whereas secondary brain tumors develop from a cancer that originates somewhere else in the body and then spreads to the brain. Primary brain tumors are rare. For example, primary gliomas of the central nervous system (CNS) account for < 2% of cancers. However, brain tumors are devastating to the patient. Everyday 27 new patients are diagnosed with a brain tumor in Canada and it is estimated that approximately 55,000 Canadians are living with brain tumors today (braintumour.ca). In Canada, brain tumors represent the leading cause of death among children under the age of 20 and are the major cause of death in young adults.

Approximately 20,000 new cases are diagnosed each year in the United States alone [2,3]. The World Health Organization (WHO) has described 120 types of brain and central nervous system (CNS) tumors (National Brain Tumor Society). Depending on their origin and characteristics, the WHO classifies brain tumors from least aggressive to most aggressive. Gliomas are the most aggressive (malignant) of CNS tumors arising from glial cells or their precursors [4,5]. The WHO further classifies gliomas into grade I-IV, with I being the least malignant and IV being the most malignant. Glioblastoma Multiforme (GBM) is a WHO grade IV glioma [5,6] and is the most common primary CNS tumor (abta.org) in European countries [7,8]. As glioblastomas are generally located in the cerebral hemispheres, they may adversely affect the control center for speech, motion, reading, writing, and executive function, thereby decreasing quality of life.

1.3 Disease Pathology and symptoms

Glioblastoma is characterized by the presence of hypoxic regions, high proliferation of tumor cells, necrosis, and extensive angiogenesis (formation of new blood vessels from existing ones). Hypoxic regions in the tumor occur due to inadequate development of vasculature [9]. Proliferation is governed by genetic mutation and multiple cell signaling pathways that control the expression of growth factors. The glioblastomas that occur in younger patients have shown gene mutations that are different from the gene mutations in glioblastomas that occur in elderly patients [10]. Glioblastomas that occurs in younger patients may have altered or deleted p53. The p53 gene is also known as tumor protein 53 (Tp53), and encodes a protein that regulates the cell cycle [10]. In contrast, glioblastomas in elderly patients have shown mutations in the phosphatase and tensin homolog (PTEN) gene that is required for the production of the PTEN protein [11]. This protein regulates the cell cycle and is responsible for keeping cells from growing and dividing in an uncontrolled way. It also triggers cell self-destruction and is involved in the process of cell movement (migration) and the formation of new blood vessels (angiogenesis). Glioblastomas are also known to contain a high level of microRNA-21 (miR-21); an antiapoptopic small RNA molecule [12]. They also contain a low level of microRNA-7

(miR-7), an inhibitor of the epidermal growth factor receptor (EGFR) [13,14]. EGFR is a cell surface protein that binds to epidermal growth factor to induce cell proliferation and is over expressed in many cancers including glioblastoma [15,16]. To support their extensive proliferation, glioblastomas develop a complex network of blood vessels by expressing high levels of vascular permeability factor (VPF) and vascular endothelium growth factor (VEGF) [17]. VEGF is known to increase vascular permeability by inducing structural abnormalities, opening gaps in the endothelium (biooncology.com) and negatively regulates tumor cell invasion [18]. Expression of VEGF is associated with peritumoral edema observed around glioblastomas. Pseudopalisading necrosis − accidental cell death − is also a hallmark of glioblastoma. Because apoptosis and necrosis can lead to cell removal, one may think that necrosis is desirable in controlling tumor growth, however necrosis leads to accelerated tumor growth, as the pseudopalisades surrounding necrotic regions secrete high levels of proangiogenic factors [19]**.** A human T_2-weight image demonstrating a Glioblastoma Multiforme tumor is shown in Figure 1.1
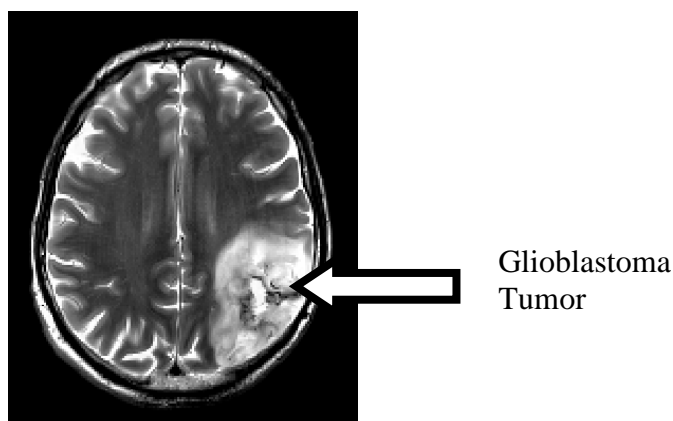
Figure 1.1 Glioblastoma Tumor-An example T_2-weighted MRI of a large glioblastoma tumor is shown in the parietal region of the human brain.

1.4 Tumor heterogeneity

The response to targeted therapy in cancer patients depends on several factors that include genotype. Genotype variation exists between patients and within a single tumor due to the development of subpopulations of cancer cells [20]. Different regions within the same tumor can have different densities of vasculature and different cellular composition. Also, tumors may exhibit differences in metabolism and necrosis [21]. At the time of clinical diagnosis, morphological and physiological features of tumor cells, such as the expression of cell surface receptors can vary with the type of tumor [22]. Cancer cells that proliferate at a higher rate require more nutrients. To meet this demand, cancer cells overexpress angiogenic factors such as VEGF and angiogenin [23]. However, tumor cells proliferate more quickly than the vasculature can develop. As a result the developed vasculature is disorganized and is not able to meet the needs of the proliferating cells. Cancer cells in the tumor core often lack proper circulation and are more hypoxic than the cancer cells in the tumor periphery [24]. The unusually developed vasculature may cause differences in drug delivery to different parts of a tumor. Tumor heterogeneity may explain variations in the uptake and cytotoxicity of chemotherapy drugs [25].

1.5 pH regulation in Tumors

The genetic mutations described above and higher rate of glycolysis lead to a distinguishing feature of malignant tumors, which is higher (alkaline) intracellular pH (pH_i) and lower (acidic) extracellular pH (pH_e). The pH is defined as the negative log of H^+ concentration. Under physiological conditions cells maintain their pH_i around 7.0 [26,27] and pH_e around 7.4. Regulation of this pH homeostasis is important for proper execution of normal cell function. Deviation from this homeostasis may contribute to the pathological changes involved in tumor growth. Specifically, in tumors, pH_i is alkaline ~7.3 [28,29] and pH_e is relatively acidic (around 6.7-7.1). A lower pH_e triggers tumor cell invasion and migration. A higher pH_i is permissive of increased cell proliferation and evasion of apoptosis [30]. In the presence of oxygen, normal cells convert glucose into

carbon dioxide, which then increases the rate of oxidative phosphorylation to maximize ATP production by mitochondria while keeping lactate production minimal. Normal cells only produce higher amounts of lactate when oxygen supply is inadequate. The process by which this happens is called anaerobic glycolysis; an inefficient way to produce energy/ATP. In contrast, cancer cells produce large amounts of lactate *even in the presence of sufficient oxygen* and therefore cancer metabolism is referred to as aerobic glycolysis. Due to extensive angiogenesis, tumor cells normally have a good supply of glucose through the circulating blood and therefore have an increased rate of aerobic glycolysis. Otto Warburg was the first to realize this deviation from normal metabolism in tumor cells, which is now known as the "Warburg effect"[31]. The pathways used for energy production/ ATP production by normal cells and tumor cells under aerobic and anaerobic conditions is summarized in Figure 1.2.
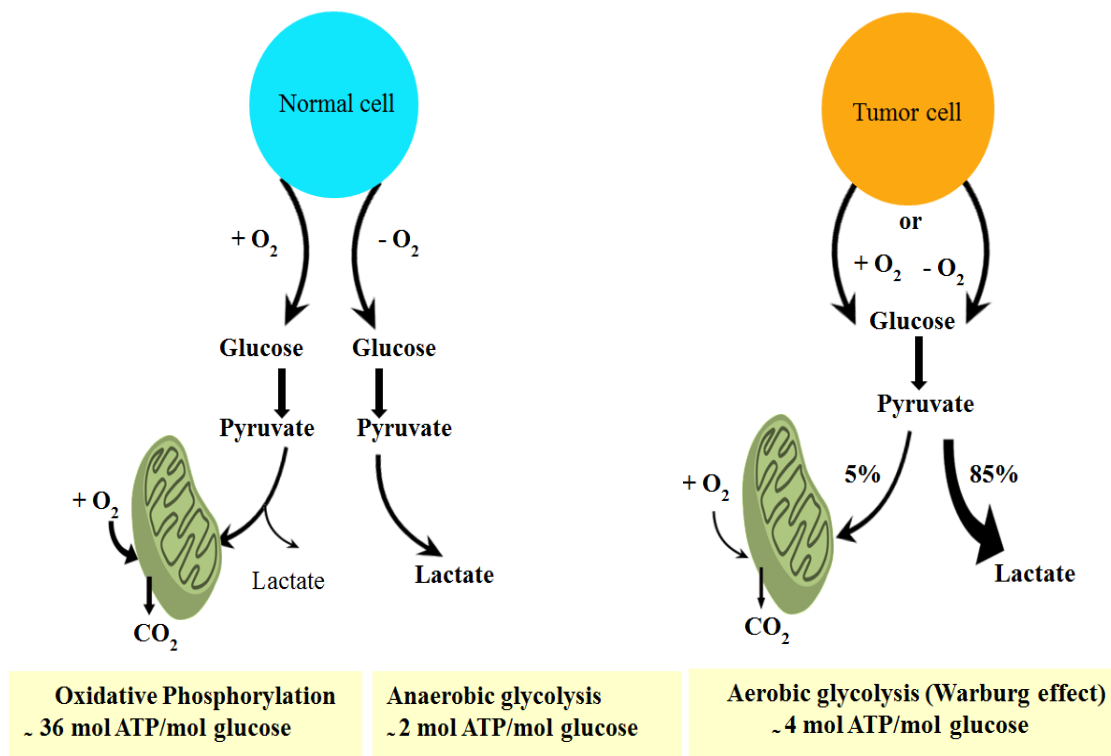
Figure 1.2 Schematic representations of the metabolic pathways in normal and tumor cells. Adapted from Matthew G. et al. [2009, Reference 25]. In the presence of oxygen, oxidative phosphorylation is the primary path to generate ATP. Normal cells undergo anaerobic glycolysis (conversion of pyruvate to lactate) only in the absence of oxygen or when the oxygen source is not sufficient. Warburg observed that tumor cells undergo aerobic glycolysis (conversion of most of the pyruvate to lactate) regardless of whether oxygen is present or absent.

Under physiological conditions glycolysis creates acid/protons (H^+). This cell-generated acid has to be extruded to maintain a normal intracellular pH. This transport is performed by "acid extruders" that move H^+ out of the cell (efflux) or move HCO_3^- into the cell (influx) resulting in an increased pH_i [32]. In addition, "acid loaders" can move H^+ into the cell or HCO_3^- out of the cell to decrease pH [32]. The most common acid loading transporters are anion exchangers, which exchange extracellular Cl^- for intracellular HCO_3^- [33] and Na^+ dependent bicarbonate transporters operating in 1:3 stoichiometry [32]. Acid extruding transporters include Na^+ dependent HCO_3^- exchangers operating in 1:2 stoichiometry, Na^+/H^+ pumps, and Na^+ dependent Cl^-/HCO_3^- exchangers [32-34].

Tumors have elevated production of H^+ due to their higher glycolytic rates and therefore we would expect to see an acidic intracellular pH_i [24]**.** However, in tumors, the excess protons that are produced are extruded by the combined action of acid extruding ion transport channels and the CO_2/ HCO_3^- buffer, which is activated in tumors and plays a major part in maintaining the higher pH_i [35]. However, the increased expression or activity of plasma membrane channels and ion transport channels that facilitate H^+ efflux and HCO_3^- influx directly or through the CO_2/HCO_3^- buffer pair overcompensate and produce a higher pH_i and lower pH_e. The buffer resists the change in pH following the addition of basic or acidic components. So to maintain a favorable alkaline pH in the face of excessive proton production in tumors, CO_2 exits the cell and dehydrates to form HCO_3^- and H^+ in the extracellular space ($CO_2 + H_2O \leftrightarrows HCO_3^- + H^+$). The HCO_3^-, generated in the extracellular space is taken up into the cells where it reacts with intracellular H^+ to form CO_2, which will again exit the cell to complete acid removal. Along with Na^+/H^+ exchangers, which are over-activated in tumors, the CO_2/HCO_3^- buffer

plays a major part in maintaining the higher pH_i. The role of 'acid extruders' and 'acid loaders' is shown in Figure 1.3.

The roll of the CO_2/HCO_3^- buffer is to shuttle H^+ within cells. Titration of intracellular acid with extracellular HCO_3^- taken up into the cell by acid extruders produces CO_2. CO_2 is freely membrane permeant and exits the cell to complete acid extrusion [21,36,37]. For effective regulation of pH_i by this system, efflux of CO_2 has to be in equilibrium with influx of HCO_3^- (1:1 stoichiometry). To keep this system in equilibrium the tumor over-expresses the carbonic anhydrase (CA) isozyme and the Aquaporin (AQP) water channel [38]. So far, about 16 humans CAs have been identified, some of which are extracellular and some of which are intracellular [39-41].
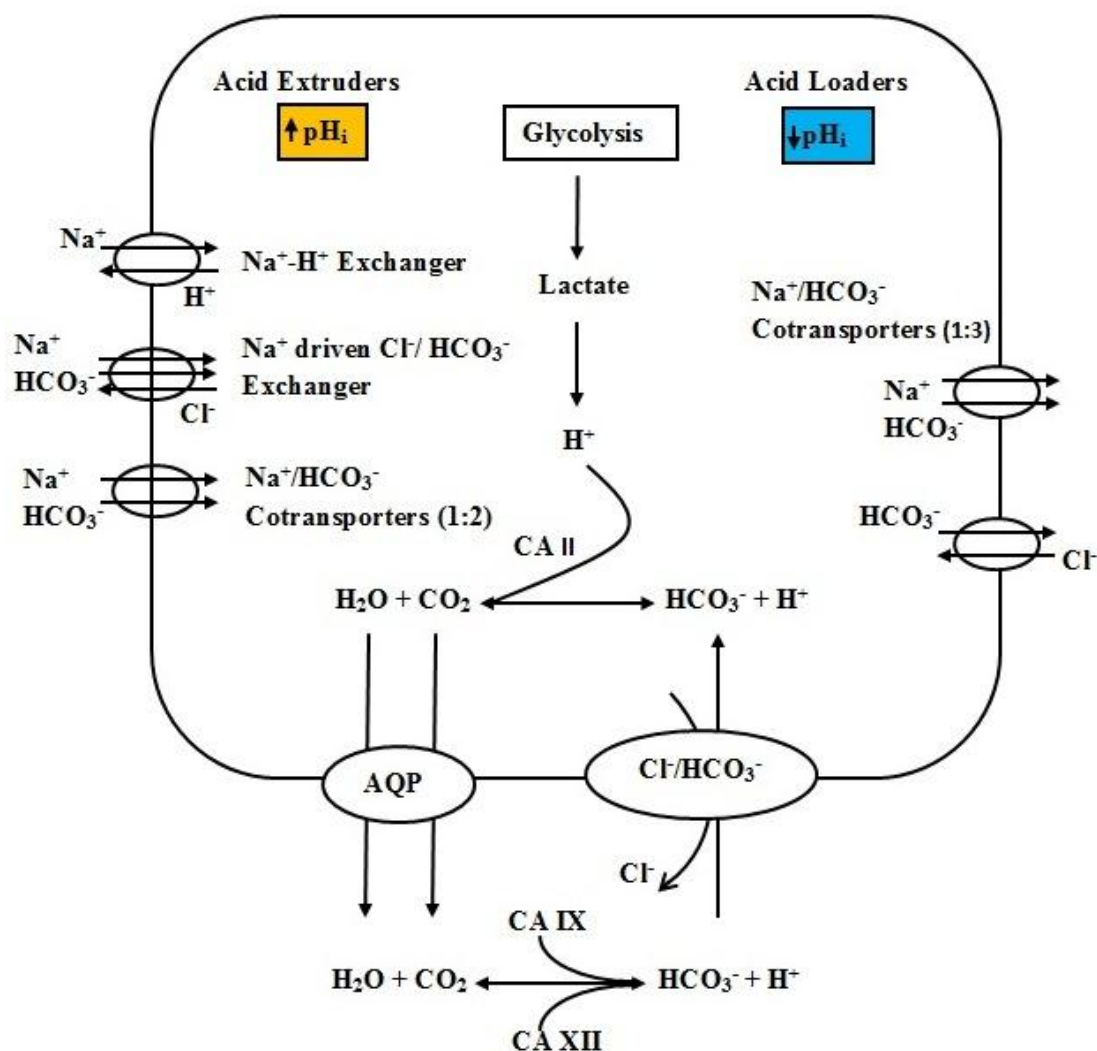
Figure 1.3 pH control mechanisms of cancer cells. In tumors, the rate of aerobic glycolysis is elevated due to increased cell proliferation. The aerobic glycolysis produces increased lactate and protons. To extrude these, tumor cells increase the expression of acid extruding ion transport channels such as the Na^+/H^+ exchangers, sodium driven Cl^-/HCO_3^- transporters and Na^+/HCO_3^- cotransporters. To further aid in acid extrusion cancer cells also increase the expression of CAII, CAIX, CAXII and the AQP1 water channels. CAII catalyzes the reaction of H^+ with HCO_3^- in the intracellular space to produce H_2O and CO_2 ($H_2O+CO_2 \leftarrow H^+ + HCO_3^-$). Then AQP1 facilitates the transport of this H_2O and CO_2 into the extracellular space where CAIX and CAXII catalyze the hydration of CO_2 to form H^+ and HCO_3^- ($H_2O + CO_2 \rightarrow HCO_3^- + H^+$). The HCO_3^- generated in the extracellular space is then taken up into the intracellular space where it again reacts with intracellular H^+ with the aid of CAII and forms H_2O and CO_2. Now this H_2O and CO_2 again get extruded in the extracellular space to complete acid removal. In cancer cells,

this process involving CAs and ion transport channels overcompensates for the increased production of acid (H^+) and produces a slightly alkaline intracellular pH, which is necessary for their survival and proliferation. Adapted from Boron 2004 [26] and Yasuhiko Hayashi *et al.* 2007 [42].

CA_s are a group of enzymes that catalyze the interconversion of CO_2 and H_2O to HCO_3^- and H^+ $(CO_2 + H_2O \leftrightharpoons HCO_3 + H^+)$ to keep CO_2/HCO_3^- in equilibrium [41,42]. The direction of the reaction depends on the form of protons, CO_2 or HCO_3^- that predominates [43]. So far thirteen human AQP have been discovered [44]. AQP are the water selective transmembrane transport channels that facilitate CO_2 transport across the membrane [45,46]. CO_2 plays a crucial role in the acidification of the tumor microenvironment [47,48]. So it is reasonable to speculate that AQP expression could contribute to the maintenance of pH balance in solid tumors by facilitating CO_2 movement and by providing the substrate for catalytic activity of extracellular CAs. Malignant glioblastomas express the carbonic anhydrases CAII, CAIX and CAXII, as well as the AQP1 channel [47]. CAII is expressed in the intracellular space whereas CAIX and CAXII are expressed in the extracellular space. CAIX is the most active isoform of carbonic anhydrase for the carbon dioxide hydration reaction [49]. Located in the extracellular space at the cell membrane, CAIX activity contributes to extracellular acidification of the tumor micro environment [50,51] and also plays an important role in maintaining amore alkaline pH_i. Previous work has shown that CAIX facilitates CO_2 extrusion and CO_2 hydration in the extracellular space, which acidifies the extracellular environment and provides a substrate for intracellular alkalinization [43,51]. Overexpression of these isoforms in many tumors including glioblastoma is associated poor survival [52,53], cancer progression, and poor response to therapy. CAXII is another extracellular tumor CA isozyme [54,55]. CAXII activity may compliment CAIX activity to facilitate CO_2 extrusion in the extracellular space and regulate acidic extracellular and alkaline intracellular pH [43,56]. CAII catalyzes the diffusion of intracellular H^+ with HCO_3^-, which is taken up in the intracellular space (cytoplasm) by the sodium-driven Cl^-/HCO_3^- exchanger or sodium bicarbonate cotransporters $(Na^+$-

HCO_3^- cotransporters), producing H_2O and CO_2 [43,44]. Several pH regulation mechanisms in tumor cells are summarized in Figure 1.4. The red box highlights the role of intracellular CA, extracellular CA and the AQP1 water channel in tumor pH regulation.
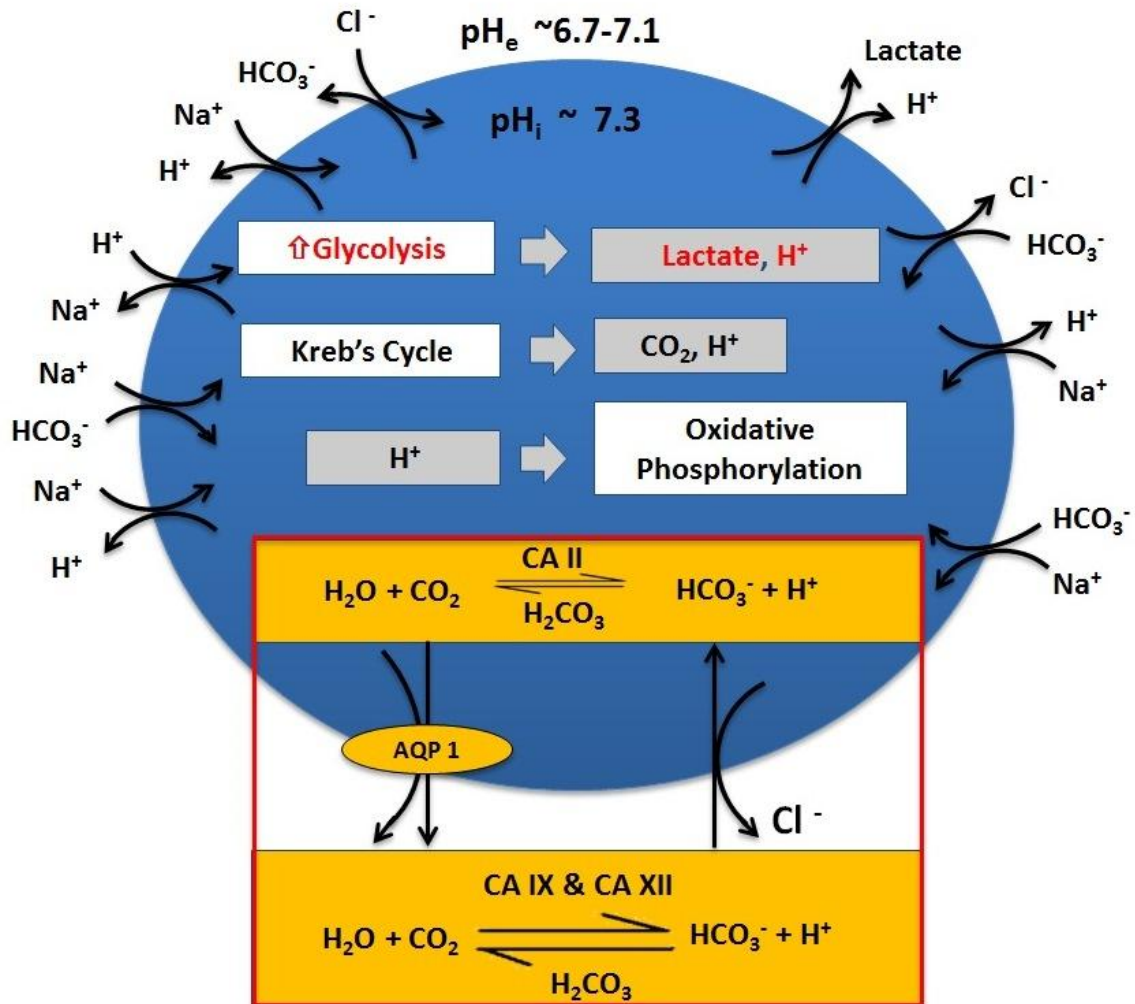
Figure 1.4 The roll of CA and AQP1 in tumor pH regulation. In tumor cells aerobic glycolysis is elevated causing increased production of lactate and H^+. This overproduction would normally lead to acidic an intracellular pH. However, cancers cells adaptively increase the expression of membrane ion transport channels to extrude the intracellular H^+ into the extracellular space. Also, to balance the acid load, the activity of CAII, CAIX, CAXII, and AQP1 increase in cancer cells (red box).

1.6 Tumor Detection

Exogenous Contrast: Tumors develop extensive microvasculature which is leaky. Many tumor diagnostic methods exploit these micro vascular changes to identify and monitor tumor growth. These methods often involve intravenous injection of an exogenous contrast agent. Depending on the molecular size and its charge, a contrast agent either remains in the vasculature or enters the cells.

Dynamic contrast enhanced MRI (DCE-MRI) involves serial acquisition of MR images before and after intravenous injection of a contrast agent, and is one of the most acceptable exogenous contrast agent methods used clinically. DCE-MRI typically uses the gadolinium based contrast agent, Gd –DTPA [23,57]. Through the bio-distribution of the agent, properties of the underlying tissues can be determined. In normal brain tissues the blood brain barrier is intact and the agent remains in the vasculature. However in tumors, where the vasculature is leaky the contrast agent can accumulate [58]. The gadolinium based contrast agents reduce the longitudinal relaxation time, T_1, of local water molecules resulting in an increase in the MRI signal on T_1-weighted images. This increase in signal is related to the concentration of agent. By fitting dynamic DCE-MRI data to an appropriate pharmacokinetic model, physiological parameters related to tumor vasculature such as vessel permeability and tissue perfusion can be determined [59]. For example, a quantitative DCE-MRI study in patients with breast cancer receiving longitudinal neoadjuvant chemotherapy showed decreased perfusion within these tumors after therapy [60].

Other contrast agents modify the magnetic susceptibility of the tissue, which reduces the local measured transverse relaxation time (T_2*). These agents stay within the vasculature - therefore they are mostly used to characterize blood vessel size and volume. Receptor targeted contrast agents are also widely used for molecular imaging of tumors as cell surface receptors are upregulated on tumor cells and endothelial cells within the tumor vasculature [61]. Also, there is a growing interest in developing chemical exchange saturation transfer (CEST) contrast agents for MRI. These agents have exchangeable

protons, which can transfer magnetization to bulk water after irradiation at their specific absorption frequency. This decreases the observed water signal intensity creating contrast between tissues of interest. Recently a PARACEST agent was used to detect glioma in a mouse model [62,63].

Similar to DCE-MRI, positron emission tomography (PET) provides functional and metabolic assessment of normal and diseased tissue. PET most often uses fluorine 18-fluorodeoxyglucose (FDG) for tumor detection. This tracer of glucose consumption is effective in tumors due to increased glucose metabolism and has been proposed as an early metabolic marker of cancer treatment. However FDG uptake also increases in conditions such as infection and hyperplasia, which can result in false positives.

All these methods for tumor detection require the injection of an exogenous contrast agent or tracer and a lengthy trial process to determine if the agent is safe to use in humans. Also, there are potential issues regarding the use of approved agents, such as the requirement for high concentrations of a contrast agent to achieve adequate detection sensitivity, the bio-distribution of contrast agents in tissues other than the intended one, and the inability of contrast agents to enter into poorly perfused tumor regions, or necrotic tissue. These shortcomings have led researchers to develop endogenous contrast mechanism for different modalities.

Endogenous Contrast: Endogenous contrast mechanisms are completely non-invasive and avoid the undesirable issues associated with the use of exogenous contrast agents.

Currently, anatomical imaging is widely used by radiologists in clinics to detect tumors and monitor tumor response to treatment by observing the size and shrinkage of tumor tissue using CT [64]. However, these measurements vary between different observers due to difficulties in determining tumor boundaries. Also, tumor size is not a reliable marker of therapy response as it is influenced by the rate of regrowth. The evaluation of antiangiogenic treatment in a murine model of melanoma by Power Doppler Ultrasound using perfusion and vascularity matrices has shown a decreased rate of blood flow in

angiogenic blood vessels, 1-3 weeks after the use of antiangiogenic treatment **[65]**. But this method can't be used when the tumor is blocked by dense structures such as bone, which inhibits the penetration of the ultrasound beam.

Magnetic Resonance Imaging (MRI) of endogenous molecules has been shown to be a highly sensitive method to detect cancer, with a wide variety of contrast mechanisms available to exploit. MRI offers detailed information about anatomical changes, changes in diffusion, and tissue volume due to apoptosis [66]. Magnetic Resonance spectroscopy (MRS) can detect metabolic characteristics of cancer arising from different metabolites [67] including creatine, total choline, lactate, and *N*-acetyl aspartate. Although highly informative, the resolution of MRS is severely limited by the concentration of endogenous molecules present in the tissue. MR thermometry can be used to monitor hyperthermia and ablative therapy [68]. Diffusion weighted imaging (DWI) has been used to measure the apparent diffusion of water in different tissue compartments. An increase in the apparent diffusion coefficient after chemotherapy has been shown to indicate a positive response to the treatment [69]. Magnetization transfer (MT) is another contrast mechanism in MRI, which can modulate the observable net magnetization of bulk water protons through the interaction of these water protons with macromolecules in the tissues. The exchange of magnetization can occur by dipolar coupling or by chemical exchange [70]. MT has been shown to be sensitive to the characteristics and composition of brain tumors. The MT effect is measured by the magnetization transfer ratio (MTR) which is calculated by subtracting positive frequencies from the negative frequencies of the MT spectrum [71]. A study investigating the histological constitution of brain tumors showed significantly lower MTR for tumors than for normal tissues [72]. The amide proton transfer (APT) technique developed by Zhou *et. al.* [73], detects a decrease in the MRI water signal by selectively exciting off resonance amide protons on intracellular proteins and peptides. Zhou demonstrated that the efficacy of magnetization transfer was affected by pH, suggesting that chemical exchange saturation transfer (CEST) [73] was pH dependent.

1.7 Treatments and relevance to pH

Because the higher intracellular pH in cancer cells is thought to resist the initiation of apoptosis, selective intracellular acidification has been proposed as a potential cancer treatment [74,75]. Some studies have also shown that the thermosensitivity of tumor cells increases at lower intracellular pH [76,77]. In addition, researchers have postulated that internucleosomal DNA fragmentation, the process of inducing cell death, requires intracellular acidification [78,79]. At the same time higher intracellular pH has been shown to reduce the effectiveness of the drug cisplatin, which is commonly used in chemotherapy [80]. Also, the uptake of a therapeutic agent into the cell is affected by the pH_e/pH_i gradient. Most chemotherapy drugs are either weak acids or weak or bases. Passive diffusion of these drugs into the cells occurs mostly in their uncharged form. These drugs accumulate by diffusion into the oppositely charged compartment. Due to the effect of the pH_e/pH_i gradient in cancer cells, basic drugs accumulate in the acidic extracellular space putting them at a therapeutic disadvantage [81]. The effect of the pH_i/pH_e gradient on drug distribution is summarized in Figure 1.5.

Tumor Cell

$pH_i \sim 7.1 - 7.3$ $pH_e \leq 7.0$

Acidic drugs   Acidic drugs

Basic drugs   **Basic drugs**
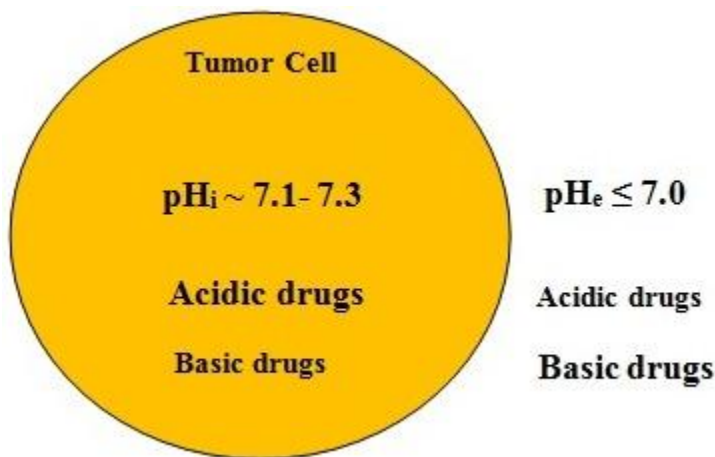
Figure 1.5 Effect of pH_e/pH_i on distribution of drugs. The font size indicates the relative concentration in that compartment. The cell membrane functions as a semi permeable structure that is permeable to uncharged drugs and tends to remain impermeable to charged drugs. As the extracellular space of tumors is acidic, the weak acid drugs remain uncharged and therefore are more easily taken into the intracellular

space. Whereas, in the acidic extracellular space weakly basic drugs becomes charged and therefore do not pass through the cell membrane [81].

The complex interaction between intracellular pH and the therapy options for the tumor motivates the use of imaging techniques like CEST which have been used in the past to generate maps of pH distribution. In addition, the selective intracellular acidification of cells is emerging as a potential enabler of cancer therapy to increase the therapeutic potential of existing drugs [82]. It is the primary goal of the work presented in this thesis to determine the pH_i lowering potential of the antiepileptic drug Topiramate in a cancer model using CEST MRI.

1.8 Modification of Tumor pH using Carbonic Anhydrase Inhibitors

1.8.1 Topiramate

Topiramate is a well-known carbonic anhydrase inhibitor (CAI) and is an anticonvulsant (antiepileptic) drug. It is approved in humans as a monotherapy or adjunctive therapy in the treatment of epileptic seizures as well as in the treatment of migraines [83]. Monotherapy doses of topiramate as high as 400 mg/day are used in humans whereas in adjunctive therapy in placebo controlled clinical trials, doses of 1000 mg/day have been used [84,85]. Epilepsy is common in patients with brain tumors and can complicate the management of these patients due to the possible interaction between antiepileptic drugs and anticancer drugs. It has been shown that Topiramate is well tolerated in patients with brain tumors associated with seizures [86]. Considering this fact, it is interesting to explore the potential metabolic effect of topiramate on brain tumors as the drug may impair the activity of tumor associated CAs which are one of the mechanisms use by tumors to maintain an elevated pH_i [87].

1.8.2 Mechanism of pH Modification

Many reports have demonstrated the over expression of intracellular CAII and extracellular CA IX and CAXII in tumors [88,89] and described their role in maintaining

higher pH_i. Topiramate has been shown to inhibit all of these CAs to some extent, however topiramate more effectively inhibits CAXII and CAII than CAIX [41].

A brief introduction to the regulation of elevated pH_i by the above mentioned CAs is given in this paragraph. In the extracellular space CAIX and CAXII catalyze the hydration of CO_2 with H_2O to produce HCO_3^- and H^+. The extracellular HCO_3^- is rapidly transported into the cell by Na^+ dependent Cl^-/HCO_3^- or Na^+ dependent bicarbonate co-transporters (1:2 stoichiometry). The intracellular HCO_3^- then reacts with intracellular H^+, lowering proton concentration (thus increasing pH_i), and producing CO_2 and H_2O by the catalytic action of intracellular CAII. This intracellular CO_2 again gets shuttled out of the cells rapidly and the cycle continues, keeping pH_i elevated [37]. The Zn^{2+} ion present in all CAs is responsible for their catalytic action. CAIs including Topiramate bind to the Zn^{2+} ion of the CAs to form a tetrahedral adduct which limits their catalytic activity [41]. A study by Leniger *et.al.,* observed a decrease in pH_i of hippocampal neurons caused by topiramate. Leniger concluded that topiramate inhibits the activity of intracellular CA and speculated that topiramate may also impair the activity of Na^+ dependent Cl^-/HCO_3^- exchange, the acid extruder, and increase the activity of Na^+ independent Cl^-/HCO_3^- exchange, the acid loader (Figure 1.3) [90].

1.9 Tumor pH measurements

1.9.1 Techniques of pH measurements

Change in pH homeostasis underlies many pathological conditions including cancer and in conditions of ischemia. Hence, many researchers are developing new techniques for pH measurement. In the past, pH electrodes were the first choice for pH measurements. However they are prone to inaccurate pH_i measurements caused by physical damage to the cells [91].

PET has also been used to measure extracellular pH of tumors in patients using the pH probe ^{11}C-labeled dimethadione (DMO) [92]. The probe is injected and the pH is

calculated from the distribution of charged and uncharged species of the probe. To measure pH using dimethadione also requires knowledge of DMO concentration in tissue water, the concentration of DMO in the extracellular space, and the volume of the intra- and extracellular spaces. The measurements of these parameters are complicated and introduce errors into the pH measurements [93,94].

Optical methods can also be used to measure pH in tumors and surrounding tissues using the fluorescent properties of optical probes [95]. There are two main optical approaches used to measure pH. The first is fluorescence ratiometric imaging microscopy, a method in which the emission spectra of the probe undergoes a pH dependent wavelength shift and pH is determined by measuring the fluorescence intensities of these spectra. However the association of the emission properties of these probes with intracellular protein and cytosolic content can introduce bias in the measurement. The second is fluorescence lifetime imaging, which measures the fluorescence decay of the pH probe, and can be used to measure pH using the pH dependent shift in fluorescence lifetime of the pH probe [95]. Several magnetic resonance (MR) methods have also been developed to measure pH of tissues. ^{31}P-Magnetic resonance spectroscopy (MRS)can be used to measure pH_i [96]. pH_i is measured from the pH dependent chemical shift of inorganic phosphate (P_i) with reference to that of phosphocreatine (PCr) [67]. However in tumors where necrotic volumes may develop, the concentration of extracellular P_i may elevate abnormally and may also contribute to the measurement making the measured pH weighted to both environments [28,97]. Extrinsic and intrinsic pH probes have also been developed for ^{1}H- MRS to measure extracellular and intracellular pH respectively. Van Sluis *et. al.* [98-100] have measured extracellular pH using the extrinsic pH probe 2- imidazole- 1- yl- 3- ethoxycarbonyl propionic acid (IEPA) in a mouse model of breast cancer. The CH_2 group resonance of IEPA is pH sensitive and therefore can be used to measure pH. The intracellular pH measurement by ^{1}H –MRS uses the pH dependent chemical shift of the two protons on the C-2 and C-4 (Im_C2 and Im_C4) resonances of the imidazole ring, of intracellular histidine but also requires administration of exogenous histidine as the endogenous concentration of this compound is too low to detect [98-100].

Hyperpolarized ^{13}C bicarbonate is another method to measure pH and involves administration of hyperpolarized $H^{13}CO_3^-$ [29,101]. This method was recently used to measure pH of lymphoma xenografts in a mouse model. The measurement showed the pH_e of lymphoma is significantly lower than that of the surrounding normal tissue. The tumor pH was measured from the voxel wise ratio of $[H^{13}CO_3^-]$ to $[CO_2]$. A similar approach has been used to map intracellular pH in the ischemic rat heart by injecting hyperpolarized $[1-^{13}C]$ pyruvate which is decarboxylated in mitochondria to form CO_2 and $H^{13}CO_3^-$ [29,101,102]. However the measurement of pH using this method requires fast imaging as the signal from hyperpolarized ^{13}C decreases rapidly. The method also suffers from limited spatial resolution.

MR relaxometry measures tissue pH by perturbing the relaxivity of bulk water protons via pH-sensitive relaxation agents such as gadolinium complexes. The pH sensitive agent GdDOTA-4AmP^5 developed by Sherry and colleagues and Aime and colleagues has been shown to have pH sensitive relaxivity [103,104]. Measurement of pH by this method requires precise measurement of agent concentration within each voxel as the relaxation also depends on the concentration. To solve this problem Raghunand *et. al.* have used serial injection of two different gadolinium agents, GdDOTA-4Amp^5 whose relaxivity is pH dependent and GdDOTP^5 whose relaxivity is pH independent. They have mapped pH_e in mouse kidneys [105] and in rat glioma [106]. With this method the pH insensitive agent is injected first. After washout of the first agent the pH sensitive agent is injected. The concentration of pH sensitive agent is determined by the distribution of pH insensitive agent and then used to measure pH_e. However this method is invasive and requires injection of exogenous contrast agents. In MRI, Chemical Exchange Saturation Transfer (CEST) is an emerging technique for measuring pH_i and has received considerable attention. The underlying principles of the CEST technique used to measure pH_i will be described in the following sections.

1.9.2 Chemical Exchange Saturation Transfer (CEST)

1.9.2.1 Origin of Nuclear Magnetic Resonance (NMR) signal

In MRI the measured signal is typically derived from the net magnetization of H^+ in bulk water. When a nucleus with spin angular momentum is placed in a magnetic field, the magnetic moments tend to align either in the direction of the magnetic field (low energy state) or in the opposite direction of the magnetic field (high energy state). At equilibrium, the number of spins in the low energy state slightly exceeds those in the high energy state and this produces a net magnetization of the system which can be thought of as a spin vector aligned with the magnetic field. Interaction between this net magnetization with an applied radio frequency pulse produces the observable signal in MRI.

1.9.2.2 Two pool proton exchange system

The concept of CEST involves the chemical exchange of protons that are present in a different chemical environment and resonate at different frequencies (ω) than bulk water protons. For the explanation of CEST, consider a two-pool system of exchanging protons. The first pool is a small pool of bound water protons (solute protons called pool A) found on intracellular proteins and peptides in tissues. The protons are rigidly bound to the surface of intracellular proteins and take a long time to change in position compared to the bulk water protons. In many cases these protons are amide or amine protons with concentration in the mM or μM range. The second pool is a large pool of free water protons (bulk water protons called pool B) with concentration about 55M as shown in Figure 1.6 below.
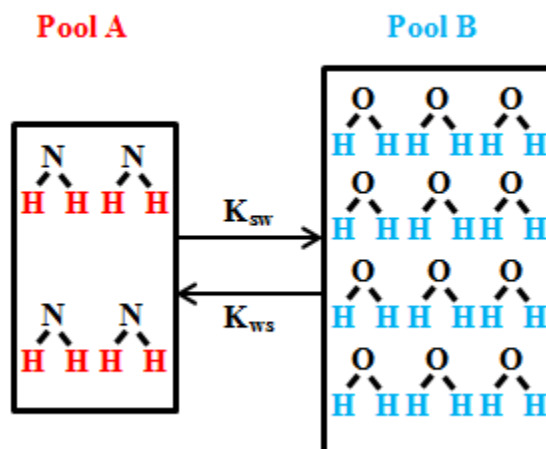
Figure 1.6 Schematic presentation of a two-pool system involved in proton exchange. The smaller pool A (solute pool) is composed of amine or amide protons associated with proteins in the tissue and the larger pool B is composed of the bulk water proton pool. The protons from the solute pool are always in chemical exchange with the bulk water protons. The process of chemical exchange depends on the concentration of the two pools and their proton exchange rates, referred to here as K_{sw} and K_{ws}.

To observe a CEST effect by MRI, the exchange rate of the proton should be in a slow to intermediate exchange regime. This means the proton exchange rates must not exceed the frequency difference ($\Delta\omega$) of the two pools i.e. K_{ws}, $K_{sw} \leq \Delta\omega$. Also, the longitudinal relaxation rate (R_1) of the solute proton pool must be slower than its exchange rate with bulk water protons. Excellent reviews describing the CEST MRI contrast mechanism have recently been published [107,108].

1.9.2.3 Saturation and Chemical Exchange

If the exchanging system of protons satisfies the above mentioned conditions, presaturation of the solute protons can modify the population of the spin energy levels of this pool. At equilibrium (before interrogation with an RF pulse) fewer proton spins are aligned in the high energy state (in the opposite direction of the magnetic field, Figure 1.7A). When a radio frequency pulse (RF) of suitable energy is applied at the offset

frequency of the solute protons, the number of solute proton spins in the high energy state increases. As the number of proton spins in low energy states decreases, the bulk magnetization of this pool will be reduced. When the number of proton spins in both energy states becomes equal the spins are said to be saturated and the net magnetization of the pool will be zero. The proton spins in the bulk water pool initially maintain their distribution according to the Boltzman Equation (Figure 1.7B). However, once the solute pool becomes saturated, the exchange of spins to the bulk water pool perturbs this equilibrium condition (Figure 1.7C). The exchange process takes place in two directions. The net effect is a reduction in the population difference between the low and high energy states in the bulk water pool. This "chemical exchange" effect results in a decrease in the net macroscopic magnetization of the bulk water pool along the z-axis. If the protons in the solute pool have a fast forward exchange rate and the saturation time is sufficiently long (in the range of seconds), the effect of the saturation of the solute pool will be to decrease the magnitude of the bulk water magnetization. This means that when a 90^0 pulse is applied to measure the magnetization, the signal intensity of the bulk water pool will be lower than with no saturation applied [107,109,110] (Figure 1.7D).
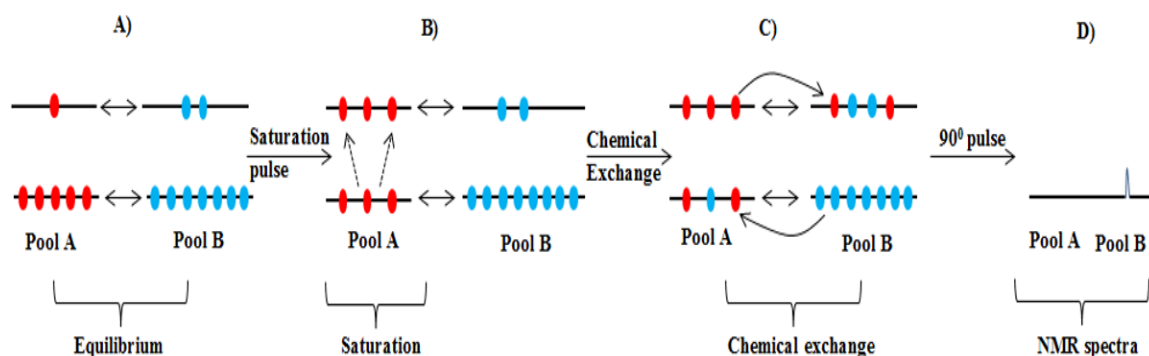
Figure 1.7 Process of saturation and chemical exchange. A) At equilibrium (before application of an RF pulse) the population of spins in the low energy state is higher than that of the population of spins in high energy state. B) When an RF saturation pulse is applied at the resonance frequency of pool B, the population of spins in the high energy state in this pool increases, which results in a decrease in net magnetization of this pool. Without exchange, the water maintains its equilibrium distribution of spins. If the RF saturation pulse is of sufficient duration then the process of saturation equalizes the

number of proton spins in the two energy levels. C) When pool B is in exchange with pool A, the magnetization from pool B is transferred to pool A. D) As a result of the transfer of energy from pool A to pool B, the signal from the bulk water pool B decreases. Adapted from reference [101]

The theory of chemical exchange has also been extended to three or four pools of exchanging protons including a pool of free (bulk water) protons and additional pools of bound protons [111,112].

1.9.2.4 Chemical Exchange and pH

The cellular environment in humans contains several different proton exchanging systems including the amide and amine protons of intracellular proteins and peptides, the hydroxyl (-OH) protons present in sugar, cellulose and glycogen, and free water protons. The rate of chemical exchange of these protons is pH dependent; exchange increases with higher pH. Recently, Zhou and coworkers used CEST contrast arising from intracellular proteins and peptides to acquire pH-weighted images of rat brain with ischemic regions and tumors. The CEST contrast was named amide proton transfer (APT) [73]. Our laboratory has also recently developed a ratiometric CEST contrast technique called Amine and Amide Concentration Independent (AACID) detection. AACID is a ratio of CEST effects arising from amide protons resonating at 3.5 ppm (parts per million) and amine protons resonating at 2.75 ppm downfield from the bulk water protons. This technique was successfully applied to measure pH changes in glioblastoma tumors after the selective acidification of the tumor environment with a drug called lonidamine [113]. However lonidamine is not currently approved for use in humans. Therefore the goal of this thesis was to apply the AACID technique to measure pH changes induced by a single dose of the drug Topiramate, which is a well-established and approved anticonvulsant.

1.9.2.5 Chemical Exchange Saturation Transfer (CEST) measurements

CEST contrast measurements are made by acquiring a spectrum called a Z-spectrum; also commonly called a CEST-spectrum. A radiofrequency saturation pulse is applied at a

predefined set of frequencies offset from the water resonance frequency. Following each application of the saturation pulse, the bulk water signal is measured. The CEST-spectrum is created by plotting the acquired bulk water signal intensity (magnetization) as a function of the applied saturation frequency. The resonance frequency of the bulk water is generally used as the center frequency and is assigned the chemical shift of 0 ppm. When the presaturation frequency is far away from the water resonance frequency, there is no direct saturation of the bulk water pool. But, if the frequency of the saturation pulse is at or close to the water resonance frequency, then the intensity of water signal decreases due to its direct saturation. This produces a negative peak in the CEST-spectrum. Similarly, if the saturation frequency is at the resonance frequency of an exchangeable solute proton pool (amide or amine), the process of saturation and chemical exchange will decrease the intensity of the bulk water signal, which will also produce a negative peak in the spectrum. In a system involving three pools of exchanging protons the CEST spectrum will have three negative peaks representing each pool. The observed CEST effect may be pH dependent. A CEST- spectrum of an exchanging system (three pool model) is depicted in Figure 1.8
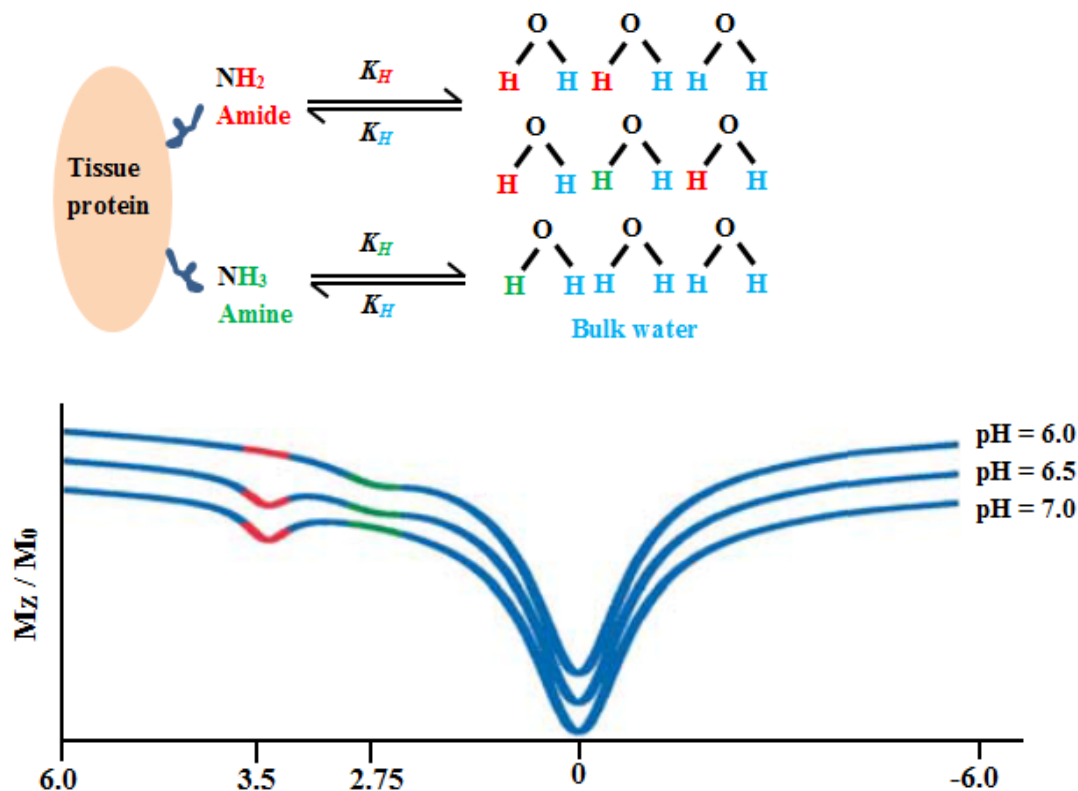
Figure 1.8 CEST spectra obtained from a three-pool proton exchanging system at different pH. When the RF saturation pulse frequency is applied far from the water resonance frequency there is no effect on the water magnetization. However when the frequency of the saturation pulse is applied at the amide resonance (3.5 ppm) or amine resonance (2.75 ppm), the process of saturation and chemical exchange decreases the signal intensity of the measured bulk water resulting in a dip in the CEST spectrum. M_0 is the bulk water magnetization without saturation and M_Z is the measured bulk water magnetization following saturation. Adapted from Ref. [114]

1.9.2.6 Water Saturation Shift Referencing (WASSR) for CEST experiments

The phenomenon of CEST exploits the transfer of magnetization from solute protons to bulk water protons. At 9.4 T, the amide protons (3.5 ppm) and amine protons (2.75 ppm) resonate relatively close to the water frequency (assigned a resonance frequency of 0 ppm). The measured change in bulk water magnetization commonly referred to as the CEST effect from amine and amide protons, is influenced by many factors including the

bulk water relaxation rate R_1, the exchange rate, the presence of magnetization transfer (MT) effects arising from immobile semisolid macromolecules (such as lipid), and B_0 inhomogeneity. Macromolecular protons have a wide absorption range 1-50 kHz and are also saturated by the off resonance RF preparation pulse. The transfer of magnetization from these protons to bulk water competes with the CEST effects from the solute proton pools of interest. Also, in vivo, CEST effects are extremely sensitive to direct water saturation. Due to the steep slope of the direct water saturation curve any inhomogeneity in the main magnetic field B_0 can shift the frequency of the water resonance in the CEST spectrum and can reduce the magnitude of the observed CEST effect.

To solve this problem Kim *et. al.* proposed a technique called Water Saturation Shift Referencing (WASSR) [115]. In WASSR a set of images is acquired ranging the RF preparation pulse frequency in small steps around the bulk water frequency using a low saturation power to reduce the MT effects and CEST effects from other exchanging systems. Polynomial fitting is then used to find the center of the Z- spectrum in each voxel.

For this study, WASSR spectra were acquired before the acquisition of each CEST spectrum by applying a saturation pulse of duration 100 ms and amplitude 0.2 µT. Each WASSR spectrum was interpolated to achieve a 1 Hz resolution and was then fitted to a polynomial to find the center peak in each voxel.

1.9.2.7 CEST - pH calibration (AACID- pH calibration)

Our group has recently developed a radiometric CEST measurement technique called Amine and Amide Concentration Independent Detection (AACID). To relate the measured AACID value to pH_i, a calibration was required. In our study, CEST spectra were acquired in normal healthy mice (N= 3) and mice with brain tumors (N=8) using the method described above. In each mouse the average AACID values were calculated directly from the B_0 corrected CEST spectra using **Equation [1]** in the normal mouse brain and contralateral region for mice with tumors, as well as within the tumor region [114].

$$\text{AACID} = \frac{M_Z\,(3.50\ ppm)\times(M_Z(6.0ppm)-M_Z(2.75\ ppm))}{M_Z(2.75\ ppm)\times(M_Z(6.0\ ppm)-M_Z(3.50\ ppm))} \qquad [1]$$

Contrast maps were also generated by calculating the contrast to noise ratio (CNR) using **Equation [2]** where $CEST_{TPM}$ represents the average CEST parameter value calculated after the TPM administration and $CEST_{Baseline}$ represents the average CEST parameter value prior to TPM treatment.

$$\text{Averege Contrast} = |\frac{\sum_{n=1}^{N}(CEST_{TPM}-CEST_{Baseline})}{\sigma_{Noise}}| \qquad [2]$$

To relate AACID values to pH, we used data from three healthy mice and eight tumor mice. In healthy mice, the whole brain AACID values were averaged. The calculated AACID values in non-tumor and tumor regions were plotted against expected pH values from the literature and the points were fitted to a linear model [114,116]. For this calibration, contralateral tissue in mice with tumors was considered to be normal. The measured AACID values in the contralateral ROIs and AACID values in normal mouse brain were assigned a $pH_i = 7.0$ [26,27] whereas, AACID values in tumor ROIs were assigned to $pH_i = 7.3$ [28,29]**.** The resulting linear relation described in **Equation [3]** was used to generate *in vivo* pH.

$$\text{AACID} = -0.34 * \text{pH} + 3.66 \qquad [3]$$

1.10 Thesis Objective

In summary, one of the features that all aggressive cancers share is higher pH_i and lower pH_e. Higher pH_i in tumors is associated with tumor growth and evasion of apoptosis [30,117] whereas lower pH_e is associated with invasive growth and cell migration [30,118]. Higher pH_i also suppresses the cytotoxic effects of alkaline anticancer drugs [119]. We hypothesize that it is possible to exploit the differences between tumor pH, healthy tissue pH, and pH regulation, for cancer detection and treatment. Specifically, in this thesis we will explore pharmacological manipulation of intracellular pH and direct monitoring of acute pH changes by MRI. For this work we have selected the antiepileptic drug Topiramate, which is approved for use in humans and has been shown to be well tolerated and effective in controlling seizures in patients with glioblastoma [86]. The objective of this thesis was to determine whether the antiepileptic drug Topiramate can modulate tumor pH and if these changes are detectable by AACID-CEST.

1.11   References

1 de Oliveira, C. et al. (2013) Understanding the costs of cancer care before and after diagnosis for the 21 most common cancers in Ontario: a population-based descriptive study. *CMAJ Open* 1 (1), E1-8

2 Modrek, A.S. et al. (2014) Brain stem cells as the cell of origin in glioma. *World J Stem Cells* 6 (1), 43-52

3 Wechsler-Reya, R. and Scott, M.P. (2001) The developmental biology of brain tumors. *Annu Rev Neurosci* 24, 385-428

4 Holland, E.C. (2000) Glioblastoma multiforme: the terminator. *Proc Natl Acad Sci U S A* 97 (12), 6242-6244

5 Dolecek, T.A. et al. (2012) CBTRUS statistical report: primary brain and central nervous system tumors diagnosed in the United States in 2005-2009. *Neuro Oncol* 14 Suppl 5, v1-49

6 Omuro, A. and DeAngelis, L.M. (2013) Glioblastoma and other malignant gliomas: a clinical review. *JAMA* 310 (17), 1842-1850

7 Kanu, O.O. et al. (2009) Glioblastoma multiforme: a review of therapeutic targets. *Expert Opin Ther Targets* 13 (6), 701-718

8 Adamson, C. et al. (2009) Glioblastoma multiforme: a review of where we have been and where we are going. *Expert Opin Investig Drugs* 18 (8), 1061-1083

9 Parks, S.K. et al. (2011) pH control mechanisms of tumor survival and growth. *J Cell Physiol* 226 (2), 299-308

10 Ishii, N. et al. (1999) Frequent co-alterations of TP53, p16/CDKN2A, p14ARF, PTEN tumor suppressor genes in human glioma cell lines. *Brain Pathol* 9 (3), 469-479

11 Tohma, Y. et al. (1998) PTEN (MMAC1) mutations are frequent in primary glioblastomas (de novo) but not in secondary glioblastomas. *J Neuropathol Exp Neurol* 57 (7), 684-689

12 Chan, J.A. et al. (2005) MicroRNA-21 is an antiapoptotic factor in human glioblastoma cells. *Cancer Res* 65 (14), 6029-6033

13 Kefas, B. et al. (2008) microRNA-7 inhibits the epidermal growth factor receptor and the Akt pathway and is down-regulated in glioblastoma. *Cancer Res* 68 (10), 3566-3572

14 Webster, R.J. et al. (2009) Regulation of epidermal growth factor receptor signaling in human cancer cells by microRNA-7. *J Biol Chem* 284 (9), 5731-5741

15 Sze, C.I. et al. (2013) Assessing current therapeutic approaches to decode potential resistance mechanisms in glioblastomas. *Front Oncol* 3, 59

16 Smith, J.S. et al. (2001) PTEN mutation, EGFR amplification, and outcome in patients with anaplastic astrocytoma and glioblastoma multiforme. *J Natl Cancer Inst* 93 (16), 1246-1256

17 Sundberg, C. et al. (2001) Glomeruloid microvascular proliferation follows adenoviral vascular permeability factor/vascular endothelial growth factor-164 gene delivery. *Am J Pathol* 158 (3), 1145-1160

18 Lu, K.V. et al. (2012) VEGF inhibits tumor cell invasion and mesenchymal transition through a MET/VEGFR2 complex. *Cancer Cell* 22 (1), 21-35

19 Kepes, J.J. (2003) Necrosis and glioblastoma: a friend or a foe? A review and a hypothesis. *Neurosurgery* 52 (5), 1242

20 Bedard, P.L. et al. (2013) Tumour heterogeneity in the clinic. *Nature* 501 (7467), 355-364

21 Hulikova, A. et al. (2011) Dual role of CO2/HCO3(-) buffer in the regulation of intracellular pH of three-dimensional tumor growths. *J Biol Chem* 286 (16), 13815-13826

22 Marusyk, A. and Polyak, K. (2010) Tumor heterogeneity: causes and consequences. *Biochim Biophys Acta* 1805 (1), 105-117

23 Wu, X. et al. (2010) Noninvasive evaluation of antiangiogenic effect in a mouse tumor model by DCE-MRI with Gd-DTPA cystamine copolymers. *Mol Pharm* 7 (1), 41-48

24 Gatenby, R.A. and Gillies, R.J. (2004) Why do cancers have high aerobic glycolysis? *Nat Rev Cancer* 4 (11), 891-899

25 Minchinton, A.I. and Tannock, I.F. (2006) Drug penetration in solid tumours. *Nat Rev Cancer* 6 (8), 583-592

26 Hubesch, B. et al. (1990) P-31 MR spectroscopy of normal human brain and brain tumors. *Radiology* 174 (2), 401-409

27 McLean, L.A. et al. (2000) Malignant gliomas display altered pH regulation by NHE1 compared with nontransformed astrocytes. *Am J Physiol Cell Physiol* 278 (4), C676-688

28   Stubbs, M. et al. (1992) An assessment of 31P MRS as a method of measuring pH in rat tumours. *NMR Biomed* 5 (6), 351-359

29   Gallagher, F.A. et al. (2008) Magnetic resonance imaging of pH in vivo using hyperpolarized 13C-labelled bicarbonate. *Nature* 453 (7197), 940-943

30   Webb, B.A. et al. (2011) Dysregulated pH: a perfect storm for cancer progression. *Nat Rev Cancer* 11 (9), 671-677

31   Vander Heiden, M.G. et al. (2009) Understanding the Warburg effect: the metabolic requirements of cell proliferation. *Science* 324 (5930), 1029-1033

32   Boron, W.F. (2004) Regulation of intracellular pH. *Adv Physiol Educ* 28 (1-4), 160-179

33   Casey, J.R. et al. (2010) Sensors and regulators of intracellular pH. *Nat Rev Mol Cell Biol* 11 (1), 50-61

34   Lee, A.H. and Tannock, I.F. (1998) Heterogeneity of intracellular pH and of mechanisms that regulate intracellular pH in populations of cultured cells. *Cancer Res* 58 (9), 1901-1908

35   Swietach, P. et al. (2010) New insights into the physiological role of carbonic anhydrase IX in tumour pH regulation. *Oncogene* 29 (50), 6509-6521

36   Lopez, M. et al. (2011) Design, synthesis, and biological evaluation of novel carbohydrate-based sulfamates as carbonic anhydrase inhibitors. *J Med Chem* 54 (5), 1481-1489

37   Swietach, P. et al. (2007) Regulation of tumor pH and the role of carbonic anhydrase 9. *Cancer Metastasis Rev* 26 (2), 299-310

38   Neri, D. and Supuran, C.T. (2011) Interfering with pH regulation in tumours as a therapeutic strategy. *Nat Rev Drug Discov* 10 (10), 767-777

39   Thiry, A. et al. (2006) Targeting tumor-associated carbonic anhydrase IX in cancer therapy. *Trends Pharmacol Sci* 27 (11), 566-573

40   Geers, C. and Gros, G. (2000) Carbon dioxide transport and carbonic anhydrase in blood and muscle. *Physiol Rev* 80 (2), 681-715

41   Supuran, C.T. (2008) Carbonic anhydrases: novel therapeutic applications for inhibitors and activators. *Nat Rev Drug Discov* 7 (2), 168-181

42   Maren, T.H. (1967) Carbonic anhydrase: chemistry, physiology, and inhibition. *Physiol Rev* 47 (4), 595-781

43   Chiche, J. et al. (2009) Hypoxia-inducible carbonic anhydrase IX and XII promote tumor cell growth by counteracting acidosis through the regulation of the intracellular pH. *Cancer Res* 69 (1), 358-368

44   Day, R.E. et al. (2014) Human aquaporins: regulators of transcellular water flow. *Biochim Biophys Acta* 1840 (5), 1492-1506

45   Endeward, V. et al. (2006) Evidence that aquaporin 1 is a major pathway for CO2 transport across the human erythrocyte membrane. *FASEB J* 20 (12), 1974-1981

46   Prasad, G.V. et al. (1998) Reconstituted aquaporin 1 water channels transport CO2 across membranes. *J Biol Chem* 273 (50), 33123-33126

47   Hayashi, Y. et al. (2007) Regulation and function of aquaporin-1 in glioma cells. *Neoplasia* 9 (9), 777-787

48   Newell, K. et al. (1993) Studies with glycolysis-deficient cells suggest that production of lactic acid is not the only cause of tumor acidity. *Proc Natl Acad Sci U S A* 90 (3), 1127-1131

49   Hilvo, M. et al. (2008) Biochemical characterization of CA IX, one of the most active carbonic anhydrase isozymes. *J Biol Chem* 283 (41), 27799-27809

50   Svastova, E. et al. (2004) Hypoxia activates the capacity of tumor-associated carbonic anhydrase IX to acidify extracellular pH. *FEBS Lett* 577 (3), 439-445

51   Swietach, P. et al. (2009) The role of carbonic anhydrase 9 in regulating extracellular and intracellular ph in three-dimensional tumor cell growths. *J Biol Chem* 284 (30), 20299-20310

52   Proescholdt, M.A. et al. (2012) Function of carbonic anhydrase IX in glioblastoma multiforme. *Neuro Oncol* 14 (11), 1357-1366

53   Haapasalo, J.A. et al. (2006) Expression of carbonic anhydrase IX in astrocytic tumors predicts poor prognosis. *Clin Cancer Res* 12 (2), 473-477

54   Brahimi-Horn, M.C. and Pouyssegur, J. (2007) Hypoxia in cancer cell metabolism and pH regulation. *Essays Biochem* 43, 165-178

55   Parkkila, S. et al. (2000) Expression of the membrane-associated carbonic anhydrase isozyme XII in the human kidney and renal tumors. *J Histochem Cytochem* 48 (12), 1601-1608

56   Chiche, J. et al. (2010) Membrane-bound carbonic anhydrases are key pH regulators controlling tumor growth and cell migration. *Adv Enzyme Regul* 50 (1), 20-33

57   Tofts, P.S. et al. (1995) Quantitative analysis of dynamic Gd-DTPA enhancement in breast tumors using a permeability model. *Magn Reson Med* 33 (4), 564-568

58   Dvorak, H.F. et al. (1988) Identification and characterization of the blood vessels of solid tumors that are leaky to circulating macromolecules. *Am J Pathol* 133 (1), 95-109

59   Tofts, P.S. et al. (1999) Estimating kinetic parameters from dynamic contrast-enhanced T(1)-weighted MRI of a diffusable tracer: standardized quantities and symbols. *J Magn Reson Imaging* 10 (3), 223-232

60   Yankeelov, T.E. et al. (2007) Integration of quantitative DCE-MRI and ADC mapping to monitor treatment response in human breast cancer: initial results. *Magn Reson Imaging* 25 (1), 1-13

61   Strijkers, G.J. et al. (2007) MRI contrast agents: current status and future perspectives. *Anticancer Agents Med Chem* 7 (3), 291-305

62   Ali, M.M. et al. (2012) A nano-sized PARACEST-fluorescence imaging contrast agent facilitates and validates in vivo CEST MRI detection of glioma. *Nanomedicine (Lond)* 7 (12), 1827-1837

63   Li, A.X. et al. (2011) In vivo detection of MRI-PARACEST agents in mouse brain tumors at 9.4 T. *Magn Reson Med* 66 (1), 67-72

64   Weber, W.A. (2009) Assessing tumor response to therapy. *J Nucl Med* 50 Suppl 1, 1S-10S

65   Gee, M.S. et al. (2001) Doppler ultrasound imaging detects changes in tumor perfusion during antivascular therapy associated with vascular anatomic alterations. *Cancer Res* 61 (7), 2974-2982

66   Sharma, U. et al. (2009) Longitudinal study of the assessment by MRI and diffusion-weighted imaging of tumor response in patients with locally advanced breast cancer undergoing neoadjuvant chemotherapy. *NMR Biomed* 22 (1), 104-113

67   Ha, D.H. et al. (2013) Application of 31P MR spectroscopy to the brain tumors. *Korean J Radiol* 14 (3), 477-486

68   Rieke, V. and Butts Pauly, K. (2008) MR thermometry. *J Magn Reson Imaging* 27 (2), 376-390

69   Cui, Y. et al. (2008) Apparent diffusion coefficient: potential imaging biomarker for prediction and early detection of response to chemotherapy in hepatic metastases. *Radiology* 248 (3), 894-900

70   Henkelman, R.M. et al. (2001) Magnetization transfer in MRI: a review. *NMR Biomed* 14 (2), 57-64

71   Zhou, J. et al. (2013) APT-weighted and NOE-weighted image contrasts in glioma with different RF saturation powers based on magnetization transfer ratio asymmetry analyses. *Magn Reson Med* 70 (2), 320-327

72   Okumura, A. et al. (1999) The characterization of human brain tumor using magnetization transfer technique in magnetic resonance imaging. *Neurol Res* 21 (3), 250-254

73   Zhou, J. et al. (2003) Using the amide proton signals of intracellular proteins and peptides to detect pH effects in MRI. *Nat Med* 9 (8), 1085-1090

74   Gottlieb, R.A. et al. (1996) Apoptosis induced in Jurkat cells by several agents is preceded by intracellular acidification. *Proc Natl Acad Sci U S A* 93 (2), 654-658

75   Nilsson, C. et al. (2006) Cytosolic acidification and lysosomal alkalinization during TNF-alpha induced apoptosis in U937 cells. *Apoptosis* 11 (7), 1149-1159

76   Lyons, J.C. et al. (1992) Modification of intracellular pH and thermosensitivity. *Radiat Res* 129 (1), 79-87

77   Song, C.W. et al. (1993) Increase in thermosensitivity of tumor cells by lowering intracellular pH. *Cancer Res* 53 (7), 1599-1601

78   Shamim, U. et al. (2012) Resveratrol-induced apoptosis is enhanced in low pH environments associated with cancer. *J Cell Physiol* 227 (4), 1493-1500

79   Barry, M.A. and Eastman, A. (1992) Endonuclease activation during apoptosis: the role of cytosolic Ca2+ and pH. *Biochem Biophys Res Commun* 186 (2), 782-789

80   Murakami, T. et al. (2001) Elevated expression of vacuolar proton pump genes and cellular PH in cisplatin resistance. *Int J Cancer* 93 (6), 869-874

81   Raghunand, N. and Gillies, R.J. (2000) pH and drug resistance in tumors. *Drug Resist Updat* 3 (1), 39-47

82   Nath, K. et al. (2013) (31) P and (1) H MRS of DB-1 melanoma xenografts: lonidamine selectively decreases tumor intracellular pH and energy status and sensitizes tumors to melphalan. *NMR Biomed* 26 (1), 98-105

83   Silberstein, S.D. et al. (2004) Topiramate in migraine prevention: results of a large controlled trial. *Arch Neurol* 61 (4), 490-495

84   Privitera, M. et al. (1996) Topiramate placebo-controlled dose-ranging trial in refractory partial epilepsy using 600-, 800-, and 1,000-mg daily dosages. Topiramate YE Study Group. *Neurology* 46 (6), 1678-1683

85   Sharief, M. et al. (1996) Double-blind, placebo-controlled study of topiramate in patients with refractory partial epilepsy. *Epilepsy Res* 25 (3), 217-224

86   Maschio, M. et al. (2008) Outcome and tolerability of topiramate in brain tumor associated epilepsy. *J Neurooncol* 86 (1), 61-70

87   Kohler, K. et al. (2007) Saccharin inhibits carbonic anhydrases: possible explanation for its unpleasant metallic aftertaste. *Angew Chem Int Ed Engl* 46 (40), 7697-7699

88   Haapasalo, J. et al. (2007) Carbonic anhydrase II in the endothelium of glial tumors: a potential target for therapy. *Neuro Oncol* 9 (3), 308-313

89   Ivanov, S. et al. (2001) Expression of hypoxia-inducible cell-surface transmembrane carbonic anhydrases in human cancer. *Am J Pathol* 158 (3), 905-919

90   Leniger, T. et al. (2004) Topiramate modulates pH of hippocampal CA3 neurons by combined effects on carbonic anhydrase and Cl-/HCO3- exchange. *Br J Pharmacol* 142 (5), 831-842

91   Tannock, I.F. and Rotin, D. (1989) Acid pH in tumors and its potential for therapeutic exploitation. *Cancer Res* 49 (16), 4373-4384

92   Rottenberg, D.A. et al. (1985) In vivo measurement of brain tumor pH using [11C]DMO and positron emission tomography. *Ann Neurol* 17 (1), 70-79

93   Kearfott, K.J. et al. (1983) C-11 dimethyloxazolidinedione (DMO): biodistribution, radiation absorbed dose, and potential for PET measurement of regional brain pH: concise communication. *J Nucl Med* 24 (9), 805-811

94   Boron, W.F. and Roos, A. (1976) Comparison of microelectrode, DMO, and methylamine methods for measuring intracellular pH. *Am J Physiol* 231 (3), 799-809

95   Hassan, M. et al. (2007) Fluorescence lifetime imaging system for in vivo studies. *Mol Imaging* 6 (4), 229-236

96   Zhang, X. et al. (2010) Tumor pH and its measurement. *J Nucl Med* 51 (8), 1167-1170

97   Ojugo, A.S. et al. (1999) Measurement of the extracellular pH of solid tumours in mice by magnetic resonance spectroscopy: a comparison of exogenous (19)F and (31)P probes. *NMR Biomed* 12 (8), 495-504

98   van Sluis, R. et al. (1999) In vivo imaging of extracellular pH using 1H MRSI. *Magn Reson Med* 41 (4), 743-750

99   Gasparovic, C. et al. (1998) A study of imidazole-based nuclear magnetic resonance probes of cellular pH. *Anal Biochem* 261 (1), 64-72

100   Vermathen, P. et al. (2000) Administration and (1)H MRS detection of histidine in human brain: application to in vivo pH measurement. *Magn Reson Med* 43 (5), 665-675

101   Gallagher, F.A. et al. (2011) Imaging pH with hyperpolarized 13C. *NMR Biomed* 24 (8), 1006-1015

102   Schroeder, M.A. et al. (2010) Measuring intracellular pH in the heart using hyperpolarized carbon dioxide and bicarbonate: a 13C and 31P magnetic resonance spectroscopy study. *Cardiovasc Res* 86 (1), 82-91

103   Lowe, M.P. et al. (2001) pH-dependent modulation of relaxivity and luminescence in macrocyclic gadolinium and europium complexes based on reversible intramolecular sulfonamide ligation. *J Am Chem Soc* 123 (31), 7601-7609

104   Zhang, S. et al. (1999) A Novel pH-Sensitive MRI Contrast Agent. *Angew Chem Int Ed Engl* 38 (21), 3192-3194

105   Raghunand, N. et al. (2003) Renal and systemic pH imaging by contrast-enhanced MRI. *Magn Reson Med* 49 (2), 249-257

106   Garcia-Martin, M.L. et al. (2006) High resolution pH(e) imaging of rat glioma using pH-dependent relaxivity. *Magn Reson Med* 55 (2), 309-315

107   van Zijl, P.C. and Yadav, N.N. (2011) Chemical exchange saturation transfer (CEST): what is in a name and what isn't? *Magn Reson Med* 65 (4), 927-948

108   Kogan, F. et al. (2013) Chemical Exchange Saturation Transfer (CEST) Imaging: Description of Technique and Potential Clinical Applications. *Curr Radiol Rep* 1 (2), 102-114

109   Woods, M. et al. (2006) Paramagnetic lanthanide complexes as PARACEST agents for medical imaging. *Chem Soc Rev* 35 (6), 500-511

110   Zhou, J. et al. (2004) Quantitative description of proton exchange processes between water and endogenous and exogenous agents for WEX, CEST, and APT experiments. *Magn Reson Med* 51 (5), 945-952

111   Desmond, K.L. and Stanisz, G.J. (2012) Understanding quantitative pulsed CEST in the presence of MT. *Magn Reson Med* 67 (4), 979-990

112   Li, A.X. et al. (2008) Four-pool modeling of proton exchange processes in biological systems in the presence of MRI-paramagnetic chemical exchange saturation transfer (PARACEST) agents. *Magn Reson Med* 60 (5), 1197-1206

113   McVicar, N. et al. (2015) Imaging chemical exchange saturation transfer (CEST) effects following tumor-selective acidification using lonidamine. *NMR Biomed* 28 (5), 566-575

114   McVicar, N. et al. (2014) Quantitative tissue pH measurement during cerebral ischemia using amine and amide concentration-independent detection (AACID) with MRI. *J Cereb Blood Flow Metab* 34 (4), 690-698

115   Kim, M. et al. (2009) Water saturation shift referencing (WASSR) for chemical exchange saturation transfer (CEST) experiments. *Magn Reson Med* 61 (6), 1441-1450

116   Gerweck, L.E. and Seetharaman, K. (1996) Cellular pH gradient in tumor versus normal tissue: potential exploitation for the treatment of cancer. *Cancer Res* 56 (6), 1194-1198

117   Lagadic-Gossmann, D. et al. (2004) Alterations of intracellular pH homeostasis in apoptosis: origins and roles. *Cell Death Differ* 11 (9), 953-961

118   Matsuyama, S. et al. (2000) Changes in intramitochondrial and cytosolic pH: early events that modulate caspase activation during apoptosis. *Nat Cell Biol* 2 (6), 318-325

119   Huang, Z. and Huang, Y. (2005) The change of intracellular pH is involved in the cisplatin-resistance of human lung adenocarcinoma A549/DDP cells. *Cancer Invest* 23 (1), 26-32

Chapter 2

Topiramate Induced Acute Intracellular Acidification in Glioblastoma Multiforme Brain Tumors

Kamini Marathe, Nevin McVicar, Alex Li, Miranda Bellyou, Susan Meakin,

And Robert Bartha

Abstract: Reversal of the intracellular/extracellular pH gradient is a hallmark of malignant tumors and is an important consideration in evaluating tumor growth potential and the effectiveness of anticancer therapies. Brain tumors including Glioblastoma Multiforme (GBM) have increased expression of the carbonic anhydrase (CA) isozyme CAII, CAIX and CAXII that contribute to the regulation of intracellular pH (pH_i). The anti-epileptic drug topiramate (TPM) inhibits these tumor associated CAs and may acidify the tumor intracellular compartment. In-vivo detection of acute tumor acidification could aid in cancer diagnosis and treatment optimization. Chemical exchange saturation transfer (CEST) magnetic resonance imaging (MRI) has been used to measure tissue pH. Using a recently developed CEST-MRI method called amide/amine concentration independent detection (AACID) we have previously shown intracellular acidification caused by a single dose of lonidamine. However lonidamine is not currently approved for use in humans. Therefore the aim of the current study was to evaluate the intracellular acidification induced by single dose of the approved drug Topiramate. Brain tumors were induced in NU/NU mice by injecting 1×10^5 U87 human glioblastoma Multiforme cells into the right frontal lobe. Using a 9.4T MRI scanner AACID CEST spectra were acquired, before and after administration of TPM (dose: 120mg/kg intraperitoneal) 15 ± 2 days after tumor cell implantation. A significant average 0.12 decrease in pH_i was observed in implanted tumors one hour after TPM administration. In contrast, contralateral tissue showed no change in pH_i. These results suggest that topiramate can rapidly induce a tumor specific physiological change detectable by AACID CEST. This pH challenge paradigm could be exploited to aid in tumor detection and treatment planning.

Keywords: Carbonic anhydrase inhibitor, Topiramate, magnetic resonance imaging, chemical exchange saturation transfer, AACID, tumor, intracellular pH.

Abbreviations used: CEST-Chemical Exchange Saturation Transfer; CA-Carbonic Anhydrase; CAI- Carbonic Anhydrase Inhibitor; GBM- Glioblastoma Multiforme; AACID- Amine and Amide Concentration-Independent Detection; pH_i- Intracellular pH; TPM- Topiramate, TR-Repetition Time, TE- Echo time, ETL- Echo Train Length, FOV- field of View

2.1 Introduction

Glioblastoma Multiforme (GBM) is the most aggressive and common form of primary brain cancer accounting for < 2% of all cancers but remains one of the most lethal human malignancies [1-3]. In patients receiving standard treatment, involving surgical resection followed by aggressive adjuvant radiation therapy and chemotherapy with temozolomide, the median survival is approximately 12-18 months after diagnosis [4,5]. Despite advances in anticancer therapies, management of patients with GBM represents a severe challenge as 90% of tumors recur due to the infiltrative nature of GBM cells [6]. The therapy options for recurrent glioma are limited, reducing the survival rate to 3-6 months in these patients [7]. Identifying progression is difficult by magnetic resonance imaging [8] as morphological changes induced by anticancer therapies, such as radiation necrosis, mimic that of recurrent brain tumor [9]. Identifying a positive tumor response to treatment can also take several weeks when using conventional methods of measuring tumor size [6]. Therefore, there is a need to develop sensitive imaging techniques that can identify malignant cells and accurately characterize tumor response to treatment within a short time interval.

One of the distinguishing features of cancer cells is the reversed intracellular/ extracellular pH gradient. Tumors cells maintain a slightly alkaline intracellular pH (pH_i) compared to normal cells, whereas the extracellular pH is more acidic. Higher pH_i is permissive of increased proliferation, cell migration, and evasion of apoptosis and is also

associated with resistance to chemotherapy drugs in cancer management [10,11]. Cancer cells regulate this reversed cellular pH gradient favorable to their survival through changes in the expression of ion transport channels and the CO_2/HCO_3^- buffering system [10,12,13]. The CO_2/HCO_3^- buffering system helps to maintain acid / base balance to regulate pH_i and minimize the effect of pH_i variation in response to intracellular H^+ production or H^+ consumption. For the CO_2/HCO_3^- buffer to effectively regulate pH_i, the influx of HCO_3^- must match the efflux of CO_2 [13]. To maintain buffer system equilibrium and pH homeostasis, cancer cells over express the hypoxia inducible carbonic anhydrase (CA) isozyme-CAII, CAIX and CAXII, as well as Aquaporin water channels (AQP1) [14-17].The carbonic anhydrases are zinc enzymes and play a crucial role in pH_i regulation by catalyzing the reversible hydration of CO_2 (CO_2 + H_2O $\leftrightharpoons$ HCO_3^- + H^+) and by enhancing the efflux of CO_2 into the extracellular space [14,15,18], which is a disguised form of acid extrusion. The direction of the reaction depends on the concentration of protons, CO_2, and bicarbonate that predominates [15]. AQP1 facilitates transport of intracellularly generated CO_2into the extracellular space and thus plays an important role in pH regulation [19]. Inhibition of the carbonic anhydrases CAs, particularly by carbonic anhydrase inhibitors (CAI) has been shown to modulate pH_i *in-vitro* in tumors [20,21]. Perturbing the pH_i balance by pharmacologically manipulating these regulating mechanisms could provide a tool to rapidly assess tumor physiology and potentially predict response to specific treatments [22].

We have recently developed and applied a novel chemical exchange saturation transfer (CEST) technique called amine and amide concentration independent detection (AACID) to monitor changes in tissue pH_i. Within the physiologically relevant range, AACID values have a linear dependence on pH_i [23]. We have demonstrated tumor selective acidification using the AACID technique in a mouse model of GBM approximately 50 minutes after administration of a single dose of the anticancer drug-lonidamine (LND) [24]. However LND is not currently approved in humans. In contrast, the drug Topiramate (TPM) is widely used in humans for the treatment of epileptic seizure [25]. This drug is a sulfonamide derivative that binds to the zinc ion site necessary for catalytic

activity of CAs and acts on most CA isoforms disturbing their ability to regulate pH_i [14]. More specifically, it is been proposed that inhibition of CAs disturbs the CO_2/HCO_3^- equilibrium causing intracellular acidification [13]. Interestingly, treatment of Lewis lung carcinoma with TPM has shown a significant reduction of lung metastases, potentially due to the effect of TPM on CAs and AQP1 [26].The purpose of the current study was to measure the change in pH_i induced in GBM tumors by a single dose of TPM using AACID CEST MRI. We hypothesized that a single dose of TPM would produce tumor specific acidification detectable by CEST MRI contrast. Manipulating pH regulation in tumor cells using pharmacologic stressors, such as topiramate, may provide a sensitive tool for the detection of tumor boundaries as well as an indicator of tumor response to treatment, as the physiological response to the pharmacologic stressor varies with cell type.

2.2 Methods

2.2.1 Subjects: Eleven NU/NU mice were included in the current study. Eight of these mice were implanted with U87MG brain tumors and used to evaluate the acute effect of TPM on tumor pH_i. The remaining three NU/NU mice were used as controls to study the effect of TPM on the pH_i of normal brain tissue.

2.2.2 Chemicals: TPM ($C_{12}H_{21}NO_8S$) was purchased from Sigma-Aldrich (Aldrich, Canada) in powder form. The drug was prepared by dissolving 50 mg of TPM in 10 ml of phosphate buffered saline (PBS, pH=7.2). The solution was vortexed for 2 minutes to dissolve the drug completely. Following baseline imaging as described below, TPM was administered intraperitoneal (i.p.) at a dose of 120 mg/kg over the course of 5 minutes using a Harvard apparatus (PHD 2000) syringe pump.

2.2.3 Mouse Tumor preparation: The human glioblastoma multiforme cell line U87MG (malignant glioma cells) was purchased from ATCC (Rockville, MD). Tumors were induced in eight NU/NU mice (10-12 weeks old, weighing 20-25 gm) as described previously [23]. Briefly, GBM cells were grown in Dulbecco's modified Eagles medium

supplemented with 10% fetal bovine serum (Wisent Inc.) at 37^0C in a humidified incubator with 5% CO_2 and passaged twice a week. Before making the final solution of 1×10^5 U87MG cells in 2ml PBS for injection, U87MG cells were washed and dissociated with phosphate buffered saline (PBS) plus 0.5 mM EDTA and then washed twice with PBS alone. Before injection of the cells, anesthesia was induced in each mouse by inhalation of 4% isoflurane in oxygen through a nosecone with the head secured in a stereotactic frame (Stoelting instruments, Wood Dale, IL, USA). Anesthetized animals were maintained using 1.5-2.5% isoflurane. The scalp was swabbed with a 3-step surgical prep and bregma was exposed by making an incision in the scalp. A 1 mm diameter hole was drilled in the skull at coordinates 1 mm anterior to bregma and 2 mm lateral from midline, to allow injection of cancer cells through a 27-guage Hamilton syringe. The U87MG cells, (2 µl), were manually injected over a 5 minute period into the right frontal lobe, 3 mm into the tissue (from bregma) with a Hamilton syringe (Reno, NV, USA) attached to a 27-gauge needle. The needle was left in place for an additional 3 minutes before withdrawing. The burr hole was covered with bone wax and the scalp was sutured closed.

2.2.4 Mouse preparation for *in-vivo* imaging: Mice were prepared for imaging 15 ± 2 days post tumor cell injection. The mice were anesthetized using 4% isoflurane in oxygen and maintained with 1.5-2.5% isoflurane in oxygen. Each mouse was positioned and secured on a custom-built MRI-compatible stage. The mouse's head was secured using a bite bar and surgical tape to minimize motion due to respiration. Mouse temperature and respiration was monitored throughout imaging. A rectal temperature probe was used to monitor temperature and a pressure transducer attached to a respiratory sensor pad was placed on the thoracic region to monitor respiration. Throughout imaging, mouse body temperature was maintained at 36.9-37.5 ^{0}C by blowing warm air over the animal using a model 1025 small-animal monitoring and gating system (SA Instruments Inc., Stony Brook, NY, USA). All animal procedures in this study were performed according to a protocol approved by the University of Western Ontario Animal Use Subcommittee. Animals were sacrificed immediately after MR imaging.

2.2.5 In-vivo Magnetic Resonance Imaging: At day 15 ± 2 after cancer cell injection, the mice were imaged on a 9.4T small animal MRI scanner equipped with a 30 mm millipede volume coil (Agilent, Santa Clara, CA, USA). Standard anatomical T_2-weighted images were used for tumor visualization. The T_2-weighted images were acquired using a 2-dimensional fast spin-echo (FSE) pulse sequence with parameters: TR/TE = 3000/10 ms, ETL = 4, effective TE = 40ms, FOV = 25.6 x 25.6 mm^2, matrix size = 128 x 128, slice thickness= 1 mm. Upon initial tumor detection, 2-slices from the T_2-weighted images with maximum tumor coverage (2 mm thickness) were selected for CEST imaging. CEST images were acquired using the FSE pulse sequence (TR/TE = 7000/7 ms, ETL = 32, effective TE = 7ms, FOV = 25.6 x 25.6 mm^2, matrix size = 64 x 64, slice thickness = 2 mm) preceded by a continuous RF saturation pulse with amplitude 1.5-µT and duration 4s. A series of fifty-five CEST images were acquired at different saturation frequencies (from 1.6 to 4.5 ppm with step size = 0.1 ppm, from 5.4 to 6.6 ppm with step size =0.1 ppm, as well as-1000 and 1000 ppm reference images. CEST images were acquired three times before and three times beginning immediately after drug injection and averaged to improve signal-to-noise ratio. For B_0 correction, the water saturation shift referencing (WASSR) technique was used [27]. Linearly spaced 37-point WASSR CEST spectra were acquired with saturation frequencies ranging from -0.6 to 0.6 ppm using the same pulse sequence except preceded by a short RF pulse (100 ms) with low amplitude (0.2 µT). Each WASSR spectrum and CEST spectrum was interpolated to a 1-Hz resolution. The CEST spectrum for each pixel was then frequency shifted, using the corresponding WASSR spectrum, to account for regional B_0 variation. A single pre- and a single post-injection CEST spectrum were created by averaging the three CEST spectra acquired before and after drug injection, respectively. A B_1 field map was generated using an actual flip-angle imaging (AFI) pulse sequence (TR = 20 ms, TE = 3.47 ms, echoes = 2, flip-angle = 70^0, FOV = 25.6 x 25.6 mm^2, matrix size= 64 x 64) [28]. The B_1 variation in the CEST slice was less than 5%, and as a result no B_1 correction was necessary. All CEST analyses were performed using MATLAB (Mathworks, Natick, MA, USA). AACID values were calculated directly from the B_0 corrected CEST spectra using Equation [1] as previously described [23,24]. AACID values were calculated on a

voxel by voxel basis directly from the CEST spectra acquired at baseline and after TPM injection within manually defined regions of interest (ROIs) within the tumor and on the contralateral side.

$$\text{AACID} = \frac{M_Z\,(3.50\;ppm) \times (M_Z(6.0ppm) - M_Z(2.75\;ppm))}{M_Z(2.75\;ppm) \times (M_Z(6.0\;ppm) - M_Z(3.50\;ppm))} \qquad [1]$$

To assess the magnitude of the change in CEST signal after treatment, a contrast to noise ratio (CNR) map was produced using Equation [2] below, where $\text{CEST}_{Baseline}$ represents a CEST parameters (AACID and pH) measured before TPM treatment, CEST_{TPM} represents CEST parameters (AACID and pH) measured after TPM treatment, and the background noise (σ_{Noise}) represents the standard deviation of a CEST parameter measured in the contralateral region before TPM treatment (N= the number of animals)

$$\text{Averege Contrast} = \left| \frac{\sum_{n=1}^{N}(\text{CEST}_{TPM} - \text{CEST}_{Baseline})}{\sigma_{Noise}} \right| \qquad [2]$$

2.2.6 AACID- pH calibration: To improve interpretation of the results, pH_i was approximated from the AACID values using a linear approximation. To calibrate pH_i, average CEST spectra were obtained within tumor and contralateral tissue *in vivo* (N=8) using the method described above. The measured AACID values for each tissue type were plotted against the expected pH values in corresponding regions (pH = 7.0 in contralateral brain tissue [29-31], pH =7.3 in tumor tissue [32-34]). The pH value assigned to tumor ROI reflects the pH value measured in hepatoma and mammary sarcomas in rat models using ^{31}P-MRS. The best-fit linear relation was used to relate AACID values to *in vivo* pH_i.

2.2.7 Statistical Analysis: AACID and pH values were calculated at baseline and following injection of TPM, within contralateral and tumor ROIs defined in each mouse brain using MATLAB. The ROIs containing tumor tissue and contralateral tissue were drawn manually based on the signal changes observed in the T_2-weighted images. A paired t-test (Microsoft Excel 2012) was used to calculate differences in mean AACID

and pH values measured in the tumor and in contralateral ROIs before and after drug injection. A similar comparison was made in control mice using the AACID and pH values from the whole brain. For control animals a whole brain ROI was drawn manually using the standard T_2-weighted anatomical images.

2.3 Results

2.3.1 AACID- pH calibration

The AACID-pH calibration results are provided in Figure 1. The best-fit linear relation given by the blue line in Figure 1 was used to relate AACID values to *in vivo* pH_i (Equation [3]):

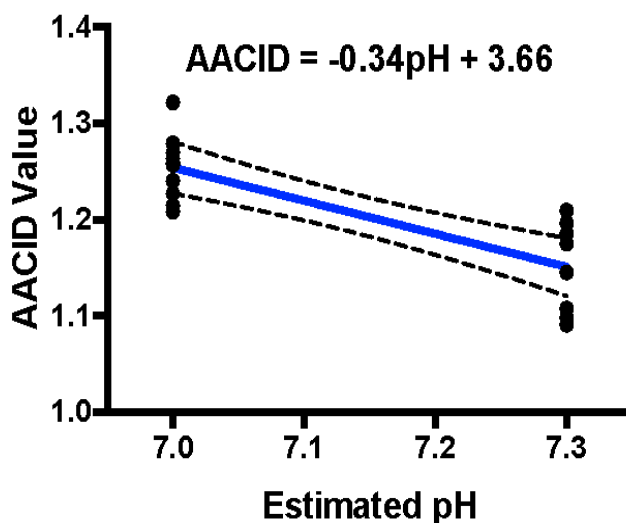$$AACID = -0.34 * pH + 3.66 \qquad\qquad [3]$$

Figure 1 AACID pH calibration. To relate AACID values to pH, AACID values in contralateral ROI were assigned to pH = 7.0, and AACID values in tumor ROI were assigned to pH = 7.3 and were fitted to linear model. The generated linear Equation was then used to generate pH maps in experimental animals.

2.3.2 CEST imaging in normal mouse brain tissue following TPM treatment

AACID maps from the brain of a control Nu/Nu mouse showed no change between the baseline scan and the scan acquired one hour after TPM injection (Figure 2a and 2b). The corresponding pH maps for the same mouse brain employing Equation [3] are also provided (Figures 2c and 2d). There were no significant differences between the mean (N=3) brain AACID CEST and pH values measured before and one hour after administration of TPM (Figure 3). Figure 2e and 2f represents the AACID and pH contrast maps employing Equation [2].
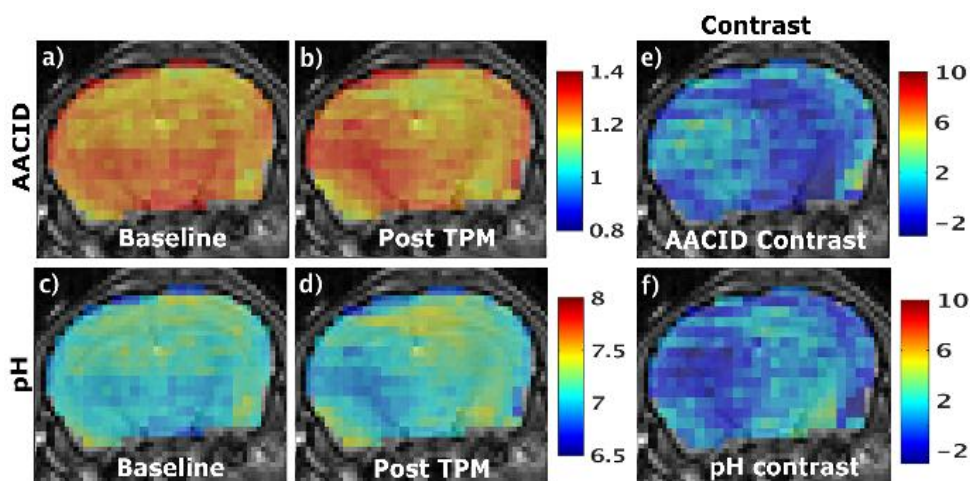

Figure 2 Representative AACID and corresponding pH maps from a healthy NU/NU mouse brain. CEST images acquired immediately before (a) and ~75 min after i.p. injection of 120mg/kg TPM (b).The corresponding pH distribution maps are provided in (c) and (d). AACID and pH values were calculated from the CEST spectra acquired at baseline and after TPM treatment using Equations 1 and 3.The AACID contrast (e) and pH contrast (f) distribution maps showed minor variations in contrast values following TPM administration.
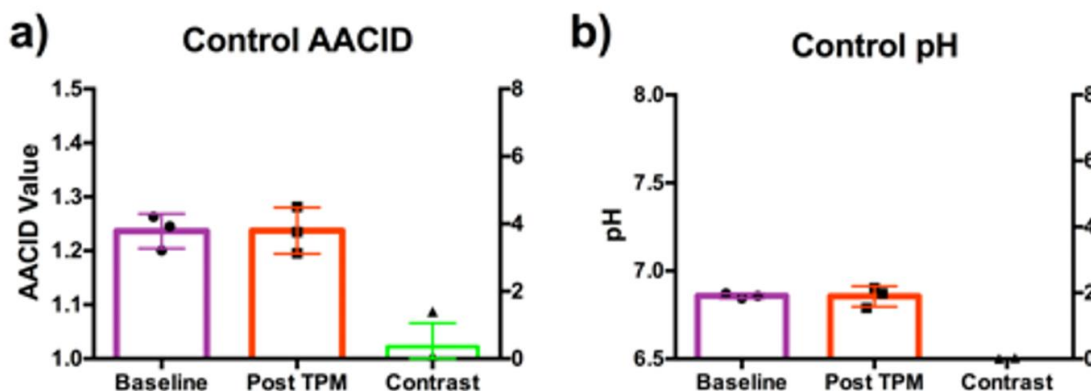
Figure 3 Summary of CEST measurements from healthy NU/NU mice (N=3). a) Mean AACID, and b) mean pH values acquired at baseline and ~75 min after 120 mg/kg TPM treatment in the whole brain. No significant differences were observed in AACID and pH values calculated before and after TPM treatment. As a result the TPM induced contrast was equal to background noise. All the error bars represent ± one standard deviation.

2.3.3 CEST imaging of U87MG brain tissue following TPM treatment

A representative anatomical T_2-weighted MR image acquired in a NU/NU mouse, 15 ± 2 days post U87MG cancer cell implantation shows typical manually defined regions of interest (Figure 4). Average CEST spectra (B_0–corrected) from one animal incorporating all pixels within the contralateral tissue ROI (Figure 5a) and tumor tissue ROI (Figure 5b) demonstrate clear differences in overall CEST effect as well as the CEST effect at 3.5 ppm. Pre injection spectra are shown in blue and post injection spectra are in shown in red (Figure 5). At baseline amine protons at 2.75 ppm did not produce any notable CEST effect in the contralateral ROI. However, amide protons resonating at 3.5 ppm generated a relatively higher CEST effect in tumor tissue compared to tissue on the contralateral side (Figure 5b). This higher amide CEST in the tumor ROI is attributed to several factors including an alkaline pH_i and increased protein content [35,36]. Topiramate had no effect on amide CEST in the contralateral ROI (Figure 5a). Conversely, changes in amide CEST effect were more pronounced in the tumor tissue ROI after topiramate administration (Figure 5b). Specifically, the amplitude of the amide CEST peak

decreased markedly following TPM administration. These results strongly suggest that TPM induced acidification, as the amide proton CEST effect decreases with decreasing pH. Quantitative AACID and pH distribution maps in one animal measured at baseline (Figure 6a, c) and 1 hour after TPM injection (Figure 6b, d) clearly show evidence of tumor selective acidification. Pre-injection (baseline) AACID distribution maps consistently showed higher AACID values on the contralateral ROI and lower AACID values within tumor ROI (Figure 6a). As expected this is reflected as higher pH values in tumor ROIs and lower pH values in contralateral ROIs (Figure 6c). Post injection AACID maps showed a marked increase in AACID values in the tumor ROI (Figure 6b) in this animal, which corresponds to a decrease in tumor pH_i (Figure 6d). The AACID and pH contrast maps generated using Equation [2] are shown in Figure 6e and 6f respectively. Figure 7 summarizes the mean AACID and pH values measured in all animals with tumors before and one hour after TPM treatment. Average AACID values did not change in the contralateral ROI (Figure 7a) after TPM injection. Conversely as expected in the tumor ROI, AACID values were significantly higher (0.045) ($p<0.05$, N=8) after TPM injection compared to baseline (Figure 7b). This corresponded to an average decrease of 0.12 pH units ($p<0.05$, N=8) after TPM injection (Figure 7d) in tumor tissue and no significant effect on pH values in contralateral ROIs (Figure 7c). The average AACID and pH CNR [mean CNR $\pm$ standard deviation] within tumor was: 1.86 ± 0.54 (AACID) and 1.85 ± 0.55 (pH), while the average AACID and pH CNR [mean CNR $\pm$ standard deviation] in contralateral tissue was: 0.12 ± 0.72 (AACID) and 0.11 ± 0.72 (pH).
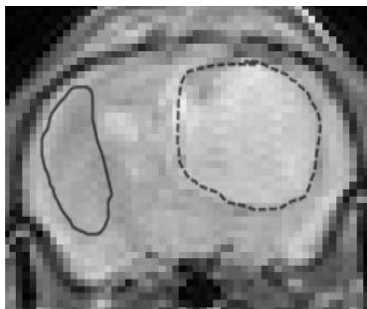
Figure 4 Standard anatomical T$_2$-weighted MR image of a mouse brain with a U87 human Glioblastoma Multiforme tumor at day 17. The hyperintense tumor region of interest (ROI) was manually drawn (dashed line) as was the contralateral ROI (solid line).
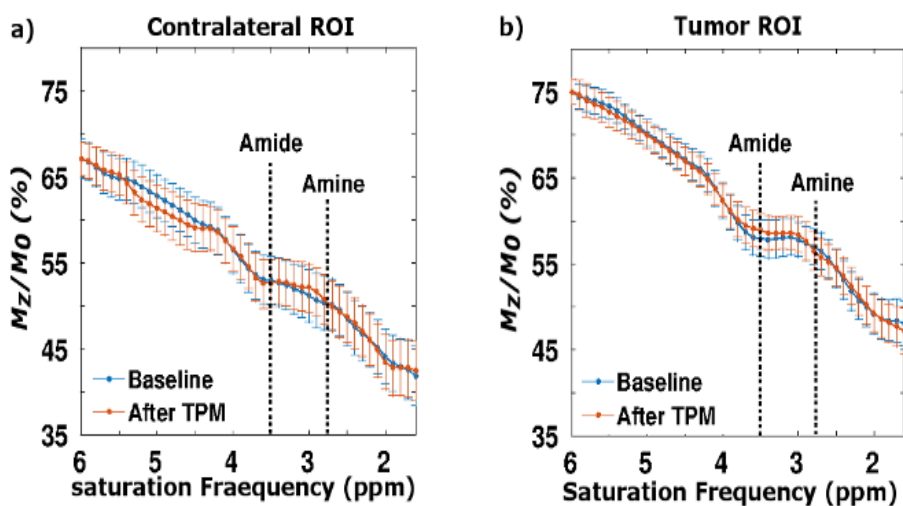
Figure 5 CEST spectra acquired in representative animal at baseline and ~75 minutes after administration of TPM. Average CEST spectra, from the ROI containing contralateral tissue (a), and from the ROI containing tumor tissue (b) with error bars equal to one standard deviation. Pre- and post- injection 6 ppm points were assigned the same values to clearly see the relative changes in amine (2.75 ppm) and amide (3.5 ppm) CEST effects.
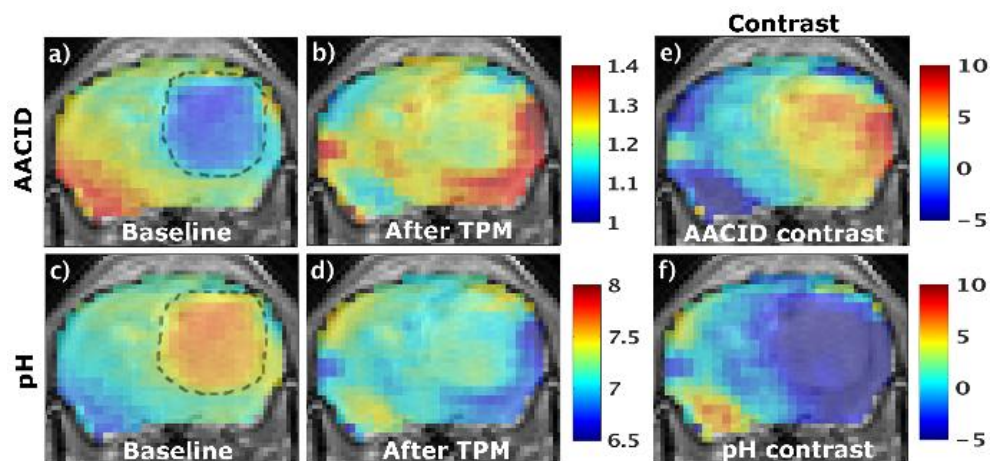
Figure 6 Representative AACID and corresponding pH maps from a NU/NU mouse brain with tumor. CEST images acquired immediately before (a) and ~75 minutes after i.p. injection of 120 mg/kg TPM (b). The corresponding pH distribution maps are provided in (c) and (d). The AACID contrast map (e) and pH contrast map (f) show changes in CEST effects following tumor selective acidification by a single dose of TPM. Tumor regions are shown in dotted lines.
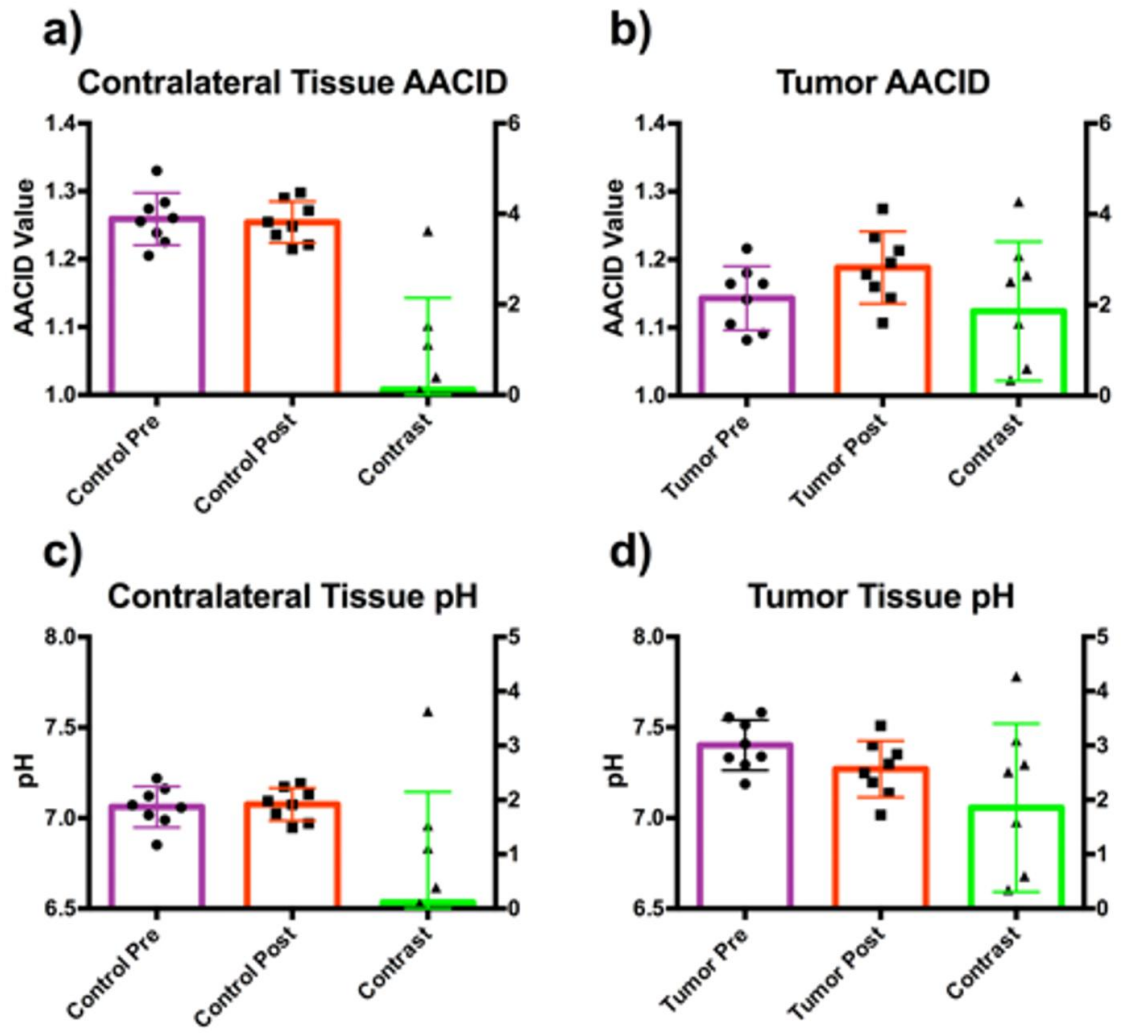
Figure 7 Summary of the CEST parameters from NU/NU mice with U87 glioblastoma brain tumors (N=8). Mean AACID (a, b) and mean pH (c, d) values acquired in contralateral ROI (a, c) and tumor ROI (b, d) with error bars equal to ± one standard deviation. The mean contrast values are also shown with error bars equal to ± one standard deviation. The mean AACID and pH values are shown at baseline (purple) and at ~ 75 min after 120 mg/kg TPM treatment (red), along with the measured contrast (green).

2.4 Discussion

The purpose of this study was to investigate whether a single dose of the drug topiramate could induce tumor selective acidification and if the decreased pH was detectable by AACID CEST MRI. Topiramate is an anticonvulsant drug that is widely used to treat epileptic seizures. Topiramate inhibits a wide range of carbonic anhydrases including tumor associated (CAII, CAIX, and CAXII). These CAs contribute to the maintenance of an alkaline intracellular pH in tumors [15]. The study herein is the first to report a significant acute decrease in tumor tissue pH measured by AACID CEST MRI following TPM injection.

Tumor cells have been associated with increased glycolysis and lactate production. To counterbalance the acidic load produced, and maintain a high pH_i that favors survival and growth [19], there is increased expression of membrane transporters such as the Na^+/H^+ exchanger, Cl^-/HCO_3^- exchangers, Na^+/HCO_3^- cotransporters, $H^+/lactate$ cotransporters, and the carbonic anhydrases CAII, CAIX and CAXII. Expression of carbonic anhydrases has been associated with poor prognosis in various human brain tumors [17,37,38]. These CAs play a vital role in maintaining an alkaline pH_i, which is permissive of cell proliferation and evasion of apoptosis. In contrast, it has previously been hypothesized that intracellular acidification could enhance apoptosis to control tumor growth [39]. For example, acidification of the intracellular compartment of melanoma xenografts has been shown to enhance the cytotoxic effect of the weakly acidic chemotherapy drug Melphalan [40]. Also, the CA inhibitor acetazolamide has shown to induce apoptosis in human cervical and renal carcinoma cell lines, *in vitro*, by inhibition of CAIX[41].In addition, the intracellular acidification of a mammary carcinoma cell line by the Na^+/H^+ inhibitor amiloride increased the effect of hyperthermia treatment [42,43]. Finally, combined silencing of CAIX and CAXII in fibroblasts decreased pH_i by 0.2 units, and tumor volume by 85% [15]. All of these studies suggest that acidification of the tumor environment could have therapeutic applications in cancer management. The sulphonamide derivative, TPM, binds to the zinc (Zn^{2+}) ion of the carbonic anhydrases,

thus inhibiting CO_2 hydration and disturbing pH regulation in tumors[12].A previous study using topiramate to treat Lewis lung carcinoma showed an inhibitory effect on tumor metastasis, potentially due to inhibition of AQP1[26].

Our group has previously demonstrated tumor selective acidification induced by a single dose of the drug Lonidamine (LND) using AACID CEST MRI. A significant increase in AACID value (0.15 units) was evident one hour after LND administration. This acidification was likely a result of decreased glycolysis and decreased lactate efflux after LND injection. In the current study the increase in AACID value (0.045 units) was considerably less than the LND induced change. One potential explanation for this difference is that LND targets the Na^+/H^+ antiport which may be a more efficient regulator of pH_i under hypoxic conditions compared to the transport of bicarbonate ions formed during the catalytic activity of CA through Cl^-/HCO_3^- transporters [44-46].

It should be noted that the pH values presented in the current study were estimated based on a calibration using pH values previously published in the brain. Some assumptions were made including: 1) the contralateral tissue in the tumor bearing animals was normal with pH_i 7.0 [30,31] and 2) the pH_i of tumor tissue was 7.3 [32-34].To develop the pH relation to AACID, AACID CEST values in glioma tumors and normal brain tissue obtained in the experimental animals were plotted against the published pH values in tumor tissue and normal tissue calculated by ^{31}P MRS. Further work is needed to calibrate the AACID- pH Equation in glioma tumors. The variability observed in the AACID and pH values (Figure 7b, d) within the tumor ROI may be due to biological variation in the animals, variation in the development of tumor vasculature in different animals, and the time of the scan (range from 13 days to17 days post cell implantation). The AACID and pH maps could also be improved in the future by increasing the signal to noise ratio of the acquired CEST images. Interestingly, we observed an increase in contrast in some regions of the contralateral brain (top and bottom left) following TPM injection (Figure 6). The phenomenon underlying this change may be related to structural and physiological changes within the tissue induced by pressure from the tumor.

Most of the studies on Topiramate and other CAIs are focused on epilepsy and other physiological conditions while only limited data are available for their use in cancer. Acetazolamide is one of the most studied CAI in cancer research and may also decrease tumor pH_i and delay tumor growth [20,47]. The results of the current study are also consistent with Leniger *et.al.*, who has suggested that changes in pH_i of hippocampal neurons can be caused by inhibition of CAs [48].

The study presented here used a small sample size; therefore this preliminary work should be repeated with more animals. The dose studied here (120mg/kg) was chosen based on the study by Bing *et. al.*,[26] as the rate of inhibition of tumor metastasis was highest at this dose. ATPM dose as high as 400mg/day has been safely used in adults in the treatment of epilepsy. The main side effect associated with the TPM treatment is acute confusion and metabolic acidosis at this dose [49]. Future work is needed to find the optimal TPM dose that produces the highest CEST effects in tumors. Future longitudinal studies are also required to evaluate the effect of long-term TPM treatment on tumor progression. Recently, many studies have shown the potential of different CAIs to control tumor growth and metastasis [50,51]. Also, the risk of having epileptic seizures in tumor patients is high, therefore investigating the use of antiepileptic drugs in cancer treatment has high translational potential [52]. Finally, other CA inhibitors should be investigated to differentiate, detect, grade and predict the outcome of possible anticancer therapies.

2.5 Acknowledgements

2.6 References

1 Kanu, O.O. et al. (2009) Glioblastoma multiforme: a review of therapeutic targets. *Expert Opin Ther Targets* 13 (6), 701-718

2 Surawicz, T.S. et al. (1998) Brain tumor survival: results from the National Cancer Data Base. *J Neurooncol* 40 (2), 151-160

3 Adamson, C. et al. (2009) Glioblastoma multiforme: a review of where we have been and where we are going. *Expert Opin Investig Drugs* 18 (8), 1061-1083

4 Parsons, D.W. et al. (2008) An integrated genomic analysis of human glioblastoma multiforme. *Science* 321 (5897), 1807-1812

5 Stupp, R. et al. (2009) Effects of radiotherapy with concomitant and adjuvant temozolomide versus radiotherapy alone on survival in glioblastoma in a randomised phase III study: 5-year analysis of the EORTC-NCIC trial. *Lancet Oncol* 10 (5), 459-466

6 Mason, W.P. et al. (2007) Canadian recommendations for the treatment of glioblastoma multiforme. *Curr Oncol* 14 (3), 110-117

7 Vredenburgh, J.J. et al. (2007) Bevacizumab plus irinotecan in recurrent glioblastoma multiforme. *J Clin Oncol* 25 (30), 4722-4729

8 Wen, P.Y. and Kesari, S. (2008) Malignant gliomas in adults. *N Engl J Med* 359 (5), 492-507

9 Kumar, A.J. et al. (2000) Malignant gliomas: MR imaging spectrum of radiation therapy- and chemotherapy-induced necrosis of the brain after treatment. *Radiology* 217 (2), 377-384

10 Webb, B.A. et al. (2011) Dysregulated pH: a perfect storm for cancer progression. *Nat Rev Cancer* 11 (9), 671-677

11 Simon, S. et al. (1994) Intracellular pH and the control of multidrug resistance. *Proc Natl Acad Sci U S A* 91 (3), 1128-1132

12 Neri, D. and Supuran, C.T. (2011) Interfering with pH regulation in tumours as a therapeutic strategy. *Nat Rev Drug Discov* 10 (10), 767-777

13 Swietach, P. et al. (2010) New insights into the physiological role of carbonic anhydrase IX in tumour pH regulation. *Oncogene* 29 (50), 6509-6521

14 Supuran et al. (2003) Carbonic Anhydrase Inhibitors. *Medicinal Research Reviews* 23 (2), 146-189

15   Chiche, J. et al. (2009) Hypoxia-inducible carbonic anhydrase IX and XII promote tumor cell growth by counteracting acidosis through the regulation of the intracellular pH. *Cancer Res* 69 (1), 358-368

16   Parkkila, A.K. et al. (1995) Immunohistochemical demonstration of human carbonic anhydrase isoenzyme II in brain tumours. *Histochem J* 27 (12), 974-982

17   Haapasalo, J. et al. (2007) Carbonic anhydrase II in the endothelium of glial tumors: a potential target for therapy. *Neuro Oncol* 9 (3), 308-313

18   Vandenberg, J.I. et al. (1996) Carbonic anhydrase and cardiac pH regulation. *Am J Physiol* 271 (6 Pt 1), C1838-1846

19   Parks, S.K. et al. (2011) pH control mechanisms of tumor survival and growth. *J Cell Physiol* 226 (2), 299-308

20   Gieling, R.G. et al. (2013) Inhibition of carbonic anhydrase activity modifies the toxicity of doxorubicin and melphalan in tumour cells in vitro. *J Enzyme Inhib Med Chem* 28 (2), 360-369

21   Parkkila, S. et al. (2000) Carbonic anhydrase inhibitor suppresses invasion of renal cancer cells in vitro. *Proc Natl Acad Sci U S A* 97 (5), 2220-2224

22   Mardor, Y. et al. (2000) Noninvasive real-time monitoring of intracellular cancer cell metabolism and response to lonidamine treatment using diffusion weighted proton magnetic resonance spectroscopy. *Cancer Res* 60 (18), 5179-5186

23   McVicar, N. et al. (2014) Quantitative tissue pH measurement during cerebral ischemia using amine and amide concentration-independent detection (AACID) with MRI. *J Cereb Blood Flow Metab* 34 (4), 690-698

24   McVicar, N. et al. (2015) Imaging chemical exchange saturation transfer (CEST) effects following tumor-selective acidification using lonidamine. *NMR Biomed* 28 (5), 566-575

25   Aggarwal, M. et al. (2013) Anticonvulsant/antiepileptic carbonic anhydrase inhibitors: a patent review. *Expert Opin Ther Pat* 23 (6), 717-724

26   Ma, B. et al. (2004) Inhibitory effect of topiramate on Lewis lung carcinoma metastasis and its relation with AQP1 water channel. *Acta Pharmacol Sin* 25 (1), 54-60

27   Kim, M. et al. (2009) Water saturation shift referencing (WASSR) for chemical exchange saturation transfer (CEST) experiments. *Magn Reson Med* 61 (6), 1441-1450

28   V.L. and Yarnykh. (2007) Actual flip-angle imaging in the pulsed steady state: a method for rapid three-dimensional mapping of the transmitted radiofrequency field. *Magn Reson Med.* 57, 192-200

29   Gerweck, L.E. and Seetharaman, K. (1996) Cellular pH gradient in tumor versus normal tissue: potential exploitation for the treatment of cancer. *Cancer Res* 56 (6), 1194-1198

30   McLean, L.A. et al. (2000) Malignant gliomas display altered pH regulation by NHE1 compared with nontransformed astrocytes. *Am J Physiol Cell Physiol* 278 (4), C676-688

31   Hubesch, B. et al. (1990) P-31 MR spectroscopy of normal human brain and brain tumors. *Radiology* 174 (2), 401-409

32   Swietach, P. et al. (2008) Cancer-associated, hypoxia-inducible carbonic anhydrase IX facilitates CO2 diffusion. *BJU Int* 101 Suppl 4, 22-24

33   Gallagher, F.A. et al. (2008) Magnetic resonance imaging of pH in vivo using hyperpolarized 13C-labelled bicarbonate. *Nature* 453 (7197), 940-943

34   Stubbs, M. et al. (1992) An assessment of 31P MRS as a method of measuring pH in rat tumours. *NMR Biomed* 5 (6), 351-359

35   Kogan, F. et al. (2013) Chemical Exchange Saturation Transfer (CEST) Imaging: Description of Technique and Potential Clinical Applications. *Curr Radiol Rep* 1 (2), 102-114

36   Zhou, J. et al. (2003) Using the amide proton signals of intracellular proteins and peptides to detect pH effects in MRI. *Nat Med* 9 (8), 1085-1090

37   Haapasalo, J.A. et al. (2006) Expression of carbonic anhydrase IX in astrocytic tumors predicts poor prognosis. *Clin Cancer Res* 12 (2), 473-477

38   Haapasalo, J. et al. (2008) Identification of an alternatively spliced isoform of carbonic anhydrase XII in diffusely infiltrating astrocytic gliomas. *Neuro Oncol* 10 (2), 131-138

39   Rich, I.N. et al. (2000) Apoptosis of leukemic cells accompanies reduction in intracellular pH after targeted inhibition of the Na(+)/H(+) exchanger. *Blood* 95 (4), 1427-1434

40   Nath, K. et al. (2013) (31) P and (1) H MRS of DB-1 melanoma xenografts: lonidamine selectively decreases tumor intracellular pH and energy status and sensitizes tumors to melphalan. *NMR Biomed* 26 (1), 98-105

41 Cianchi, F. et al. (2010) Selective inhibition of carbonic anhydrase IX decreases cell proliferation and induces ceramide-mediated apoptosis in human cancer cells. *J Pharmacol Exp Ther* 334 (3), 710-719

42 Song, C.W. et al. (1993) Increase in thermosensitivity of tumor cells by lowering intracellular pH. *Cancer Res* 53 (7), 1599-1601

43 Kim, G.E. et al. (1991) Effects of amiloride on intracellular pH and thermosensitivity. *Int J Radiat Oncol Biol Phys* 20 (3), 541-549

44 Boyer, M.J. and Tannock, I.F. (1992) Regulation of intracellular pH in tumor cell lines: influence of microenvironmental conditions. *Cancer Res* 52 (16), 4441-4447

45 Morgan, P.E. et al. (2004) Carbonic anhydrase inhibitors that directly inhibit anion transport by the human Cl-/HCO3- exchanger, AE1. *Mol Membr Biol* 21 (6), 423-433

46 Lyons, J.C. et al. (1992) Modification of intracellular pH and thermosensitivity. *Radiat Res* 129 (1), 79-87

47 Teicher, B.A. et al. (1993) A carbonic anhydrase inhibitor as a potential modulator of cancer therapies. *Anticancer Res* 13 (5A), 1549-1556

48 Leniger, T. et al. (2004) Topiramate modulates pH of hippocampal CA3 neurons by combined effects on carbonic anhydrase and Cl-/HCO3- exchange. *Br J Pharmacol* 142 (5), 831-842

49 Pierson, M.D. et al. (2010) Topiramate-induced confusion following a single ingestion of 400 mg. *Gen Hosp Psychiatry* 32 (6), 647 e641-643

50 Lou, Y. et al. (2011) Targeting tumor hypoxia: suppression of breast tumor growth and metastasis by novel carbonic anhydrase IX inhibitors. *Cancer Res* 71 (9), 3364-3376

51 Pacchiano, F. et al. (2011) Ureido-substituted benzenesulfonamides potently inhibit carbonic anhydrase IX and show antimetastatic activity in a model of breast cancer metastasis. *J Med Chem* 54 (6), 1896-1902

52 Weller, M. et al. (2012) Epilepsy meets cancer: when, why, and what to do about it? *Lancet Oncol* 13 (9), e375-382

3 Conclusions and Future Directions

In this section, limitations of the study and a brief summary of relevant findings of Chapter 2 are considered. In addition, some implications and future directions are discussed.

3.1 Limitations

There are several limitations to the current work that should be considered.

i) In the treatment of epileptic seizures, topiramate (400 mg/d) is used orally in humans. In this thesis we have used intraperitoneal (i.p.) topiramate at a dose of 120 mg/kg, which is comparatively higher than the dose used in humans. Also, although topiramate is widely used in the treatment of epilepsy there is no injectable product. However in one investigational study, it has been shown that the bioavailability of the intravenous formulation and the oral formulation is equivalent and that the intravenous formulation is well tolerated in healthy adults and adults with epilepsy, and that a single dose of intravenous topiramate can be safely administered [1-3]. However, the study presented in this thesis was not designed to optimize the topiramate dose used in humans for cancer detection.

ii) The pH values presented in this study were approximated. The AACID-pH relationship used in this study was not developed using an independent pH calibration. Rather, it was developed by equating the average AACID values measured in tumors and contralateral tissue, to published pH values from these same tissue measured using ^{31}P-MRS and assuming a linear dependence.

iii) The experiment was not designed to measure the long-term effect of topiramate on tumors. Therefore we cannot judge whether topiramate can play a role in tumor management or could be a part of the treatment regime.

iv) There was great variability in the effect of topiramate on pH_i in different animals. This variability was independent of the size of the tumor and might be related to the

expected heterogeneous vasculature in these tumors; although, this effect was not verified in this study.

3.2 Conclusions

Cancer affects millions of people world-wide [4]and many malignant forms of cancer are difficult to treat with the traditional available treatment options. The concept of exploring the use of carbonic anhydrase inhibitors in cancer treatment is increasing, in part due to their effect on pH regulation in tumors [5]. In light of several excellent reviews, we attempted to measure pH changes induced by a single dose of the CAI topiramate using the AACID CEST MRI technique [6,7]. In malignant glioblastoma tumors implanted in immune–compromised mice, the results presented indicated that topiramate decreased pH_i by 0.12 units within~75 min after administration. On average we did not observe any change in pH_i in the contralateral brain regions of mice with tumors or in the brains of healthy mice. This finding is very exciting considering that intracellular acidification of the tumor intracellular space could improve the efficacy of chemotherapy as well as hyperthermia treatment [8,9].

3.3 Future Directions

This thesis examined the effect of the carbonic anhydrase inhibitor, Topiramate, on tumor pH_i. pH is elevated in tumors and is an important contributor to tumor cell proliferation[10]. In contrast, acidification of the tumor intracellular space increases the rate of apoptosis as well as induces tumor growth delay. Many other carbonic anhydrase inhibitors have shown promise in inhibiting tumor associated carbonic anhydrases. Therefore a logical extension of this work would be to evaluate the effect of these CAI on tumor pH_i and optimize the drug that causes the greatest decrease in pH_i with therapeutic dosages. Also, it will be interesting to design longitudinal experiments to observe the effects of Topiramate on tumor growth and optimize the dose for maximum growth delay as well as treating tumors with different combination of CAI to see if they work synergistically. A well-established antiepileptic drug Valporate was proposed to have antitumor activity and has been shown to decrease tumor growth and metastasis [11].

Therefore we should examine the combined effects of drugs that have different targets to control tumor growth.

Reports on the expression of CA II in glioblastoma are scarce but have indicated that many malignant cell lines express CA II at low levels. [12-14]. In contrast, expression of CAIX and CAXII is elevated in different tumor lines including glioblastoma [12,15-17]. Topiramate is a potent inhibitor of CAII and moderate inhibitor of CAIX. CAIX has a catalytic performance rate similar to CAII. Knockdown of CAIX increased the rate of apoptotic cell death after radiation and temozolomide treatment [17]. In addition, inhibition of the CAIX carbonic anhydrase decreased the rate of metastasis in a mouse model of breast tumor [17,18]. Therefore it would be of interest to compare the effects of tumor specific CAIX inhibitors and CAII inhibitors on tumor pH_i.

Another extension of this thesis would be to measure pH_e along with pH_i to monitor the effect on extracellular pH, as it is the pH gradient across the plasma membrane that impacts the efficacy of chemotherapy drugs. This simultaneous measurement of pH_i and pH_e may aid to design the most effective and personalized treatment regime.

The results from this study indicate the potential value of carbonic anhydrase inhibitors in tumor acidification and hopefully will stimulate future experiments to expand the role of such drugs in cancer treatment.

3.4 References

1   Clark, A.M. et al. (2013) Intravenous topiramate: comparison of pharmacokinetics and safety with the oral formulation in healthy volunteers. *Epilepsia* 54 (6), 1099-1105

2   Clark, A.M. et al. (2013) Intravenous topiramate: safety and pharmacokinetics following a single dose in patients with epilepsy or migraines taking oral topiramate. *Epilepsia* 54 (6), 1106-1111

3   Glass, H.C. et al. (2011) Topiramate for the treatment of neonatal seizures. *Pediatr Neurol* 44 (6), 439-442

4   Shi, Y. and Hu, F.B. (2014) The global implications of diabetes and cancer. *Lancet* 383 (9933), 1947-1948

5   Poulsen, S.A. (2010) Carbonic anhydrase inhibition as a cancer therapy: a review of patent literature, 2007 - 2009. *Expert Opin Ther Pat* 20 (6), 795-806

6   Ma, B. et al. (2011) The effect of topiramate on tumor-related angiogenesis and on the serum proteome of mice bearing Lewis lung carcinoma. *Eur J Pharmacol* 663 (1-3), 9-16

7   Vullo, D. et al. (2005) Carbonic anhydrase inhibitors. Inhibition of the transmembrane isozyme XII with sulfonamides-a new target for the design of antitumor and antiglaucoma drugs? *Bioorg Med Chem Lett* 15 (4), 963-969

8   Gieling, R.G. et al. (2013) Inhibition of carbonic anhydrase activity modifies the toxicity of doxorubicin and melphalan in tumour cells in vitro. *J Enzyme Inhib Med Chem* 28 (2), 360-369

9   Teicher, B.A. et al. (1993) A carbonic anhydrase inhibitor as a potential modulator of cancer therapies. *Anticancer Res* 13 (5A), 1549-1556

10   Webb, B.A. et al. (2011) Dysregulated pH: a perfect storm for cancer progression. *Nat Rev Cancer* 11 (9), 671-677

11   Blaheta, R.A. and Cinatl, J., Jr. (2002) Anti-tumor mechanisms of valproate: a novel role for an old drug. *Med Res Rev* 22 (5), 492-511

12   Haapasalo, J. et al. (2007) Carbonic anhydrase II in the endothelium of glial tumors: a potential target for therapy. *Neuro Oncol* 9 (3), 308-313

13   Kivela, A.J. et al. (2001) Differential expression of cytoplasmic carbonic anhydrases, CA I and II, and membrane-associated isozymes, CA IX and XII, in normal mucosa of large intestine and in colorectal tumors. *Dig Dis Sci* 46 (10), 2179-2186

14   Parkkila, A.K. et al. (1995) Immunohistochemical demonstration of human carbonic anhydrase isoenzyme II in brain tumours. *Histochem J* 27 (12), 974-982

15   Proescholdt, M.A. et al. (2005) Expression of hypoxia-inducible carbonic anhydrases in brain tumors. *Neuro Oncol* 7 (4), 465-475

16   Ivanov, S. et al. (2001) Expression of hypoxia-inducible cell-surface transmembrane carbonic anhydrases in human cancer. *Am J Pathol* 158 (3), 905-919

17   Proescholdt, M.A. et al. (2012) Function of carbonic anhydrase IX in glioblastoma multiforme. *Neuro Oncol* 14 (11), 1357-1366

18   Lou, Y. et al. (2011) Targeting tumor hypoxia: suppression of breast tumor growth and metastasis by novel carbonic anhydrase IX inhibitors. *Cancer Res* 71 (9), 3364-3376

Appendices

PI Name: Bartha, Robert
AUP Title: Development Of Novel Targeted MRI Contrast Agents
Approval Date: 04/29/2015

Official Notice of Animal Use Subcommittee (AUS) Approval: Your new Animal Use Protocol (AUP) entitled "Development of Novel Targeted MRI Contrast Agents" has been APPROVED by the Animal Use Subcommittee of the University Council on Animal Care. This approval, although valid for four years, is subject to annual Protocol Renewal.2015-005: 1

1. This AUP number must be indicated when ordering animals for this project.
2. Animals for other projects may not be ordered under this AUP number.
3. Purchases of animals other than through this system must be cleared through the ACVS office. Health certificates will be required.

The holder of this Animal Use Protocol is responsible to ensure that all associated safety components (biosafety, radiation safety, general laboratory safety) comply with institutional safety standards and have received all necessary approvals. Please consult directly with your institutional safety officers.

CURRICULUM VITAE

Kamini Yogesh Marathe

Education

- **M.Sc. Candidate (Medical Biophysics)** (09/2013-12/2015)
  The University of Western Ontario, London, Ontario, Canada
  Thesis: Intracellular acidification in brain tumors induced by Topiramate: In-vivo detection using chemical exchange saturation transfer magnetic resonance imaging
  Supervisor: Dr. Robert Bartha

- **B.Ed.** (07/2002-04/2003)
  Navalbhau Pratishthan's Shikshanshashtra Mahavidyalaya, Amalner

- **M.Sc. (Physics)** (07/2000-06/2002)
  Pratap Collage, Amalner, North Maharashtra University, Jalgaon, Maharashtra, India
  Thesis: Microcrystalline CdS and PbS crystals by flux method
  Supervisor: Dr. L.A. Patil

- **B.Sc. (Physics)** (07/1997-06/2000)
  Pratap Collage, Amalner, North Maharashtra University, Jalgaon, Maharashtra, India
  Thesis: Studies on photo conducting properties of CdS
  Supervisor: Dr. L.A. Patil

Honors and Scholarships

- **WGRS** (Western Graduate Research Scholarship) (09/2013-12/2015)
  The University of Western Ontario, London, Ontario, Canada

- 2nd rank in M. Sc. (Physics) University Graduates (2002)
  North Maharashtra University, Jalgaon, Maharashtra, India

Experience

- **Lecturer** (07/2003-04/2004)
  Pratap Collage, Amalner

Poster Presentations

- **Kamini Marathe**, Nevin McVicar, Alex Li, Mojmir Suchy, Miranda Bellyou, Susan Meakin, Robert Bartha. Topiramate Induced Intracellular acidification in Brain Tumors. [Submitted to London Health Research Day, 04/2015]

- **Kamini Marathe**, Nevin McVicar, Alex Li, Mojmir Suchy, Miranda Bellyou, Susan Meakin, Robert Bartha. Topiramate Induced Intracellular Acidification in Brain Tumors: In- Vivo Detection using Chemical Exchange Saturation Transfer Magnetic Resonance Imaging. [Submitted to International Society For Magnetic Resonance in Medicine, 05/2015]

- **Kamini Marathe**, Nevin McVicar, Alex Li, Mojmir Suchy, Miranda Bellyou, Susan Meakin, Robert Bartha. Carbonic Anhydrase Inhibitor induced Intracellular Acidification in Brain Tumors: a Magnetic Resonance Imaging Study. [Submitted to Imaging Network Ontario, 03/2015]

- **Kamini Marathe**, Nevin McVicar, Alex Li, Robert Bartha. Optimization of pH measurements by CEST MRI at 9.4T. [Submitted to Robarts research Retreat, 06/2014]

Oral Presentation

- **Kamini Marathe**, Nevin McVicar, Alex Li, Robert Bartha. pH measurement in brain tumors.[Submitted to 3 Minute Thesis presentation, Western university, 11/2013]